# TABLE OF CONTENTS


| SECTION NO. | TITLE | PAGE NO. |
|---|---|---|
| **1.** | **INTRODUCTION** | 1 |
| | 1.1. Myocardial Infarction | 1 |
| | 1.2. Medical Technologies | 2 |
| | 1.3. Arrhythmia | 3 |
| | 1.4. Research Progress Summary | 4 |
| | 1.5. Research Findings | 5 |
| | 1.6. Proposed Model | 6 |
| **2.** | **NEED FOR THE STUDY** | 6 |
| **3.** | **RELATED WORK** | 7 |
| **4.** | **PROBLEM STATEMENT** | 9 |
| **5.** | **OBJECTIVES OF THE STUDY** | 9 |
| **6.** | **METHODOLOGY** | 10 |
| | 6.1. Preprocessing | 10 |
| | 6.1.1. Median Filtering | 10 |
| | 6.2. Segmentation | 10 |
| | 6.2.1. Morphological Filtering | 11 |
| | 6.2.2. Fuzzy C-Means | 12 |
| | 6.3. Feature Selection | 13 |
| | 6.3.1. Gray Thresholding | 14 |
| | 6.4. Feature Extraction | 14 |
| | 6.4.1. Region Growing Algorithm | 15 |
| | 6.5. Classification and Prediction | 15 |
| | 6.5.1. Decision Tree Algorithm | 16 |

**7. EVALUATION OF CLASSIFIER MODEL** 17
7.1. Feed Forward Neural Network 17
**8. RESULTS AND DISCUSSION** 18
8.1. Proposed Model 18
8.2. The Predictive Capability of IAAP 20
8.2.1. Dataset Description 20
8.2.2. Phase I 21
8.2.3. Phase II 27
8.2.4. Phase III 29
8.2.5. Phase IV 29
8.2.6. Phase V 31
8.2.7. Matrix Evaluation 31
8.2.8. Experimental Evaluation on Proposed Model Using Normal Heart 33
8.3. Statistical Evaluation 34
8.3.1. Mean Squared Error 34
8.3.2. Structural Similarity Index 36
8.3.3. Support Vector Machine Classification 38
8.3.4. K-Nearest Neighbors Classification 39
8.3.5. Decision Tree Classification 39
8.3.6. Feed Forward Neural Network Classification 41
8.3.7. Performance of the Proposed Model (IAAP) 45
8.3.8. Performance Evaluation on Systole with Ground Truth Images 46
**9. CONCLUSIONS** 48
**REFERENCES** 48
**LIST OF PUBLICATIONS** 54

# 1. INTRODUCTION

Myocardial Infarction is also called heart attack, occurs when blood flow decreases or discontinues to some part of heart, causing damage to the heart muscle and form scar tissue. The reduced blood flow occurs due to partial or complete block within the heart arteries. Complete blockage of the heart arteries leads to Myocardial Infarction (MI). MI could also potentially lead to other medical conditions such as abnormal heart rhythms, also known as arrhythmia. Medical experts measure the volume of a scar tissue to identify an arrhythmia patient. To bring about an early prediction of arrhythmia in an individual, an exact measurement of their scar tissue is utilized and the current research proposes a hybrid model for it. This hybrid model acts as a secondary tool for medical experts to identify an arrhythmia patient.

## 1.1. Myocardial Infarction

Myocardial Infarction is the blockage or narrowing of the coronary artery. Arteries and veins are designed for transporting oxygen rich blood from the heart to other parts of the human body and arteries carry back the depleted blood back to the heart. In some situations, perusal of an unhealthy lifestyle could cause fat deposition in the arteries called plaques. The rise of cholesterol composition on the walls of an artery could potentially restrict blood flow. Artery walls can rupture due to plaques and it is one of the leading causes of MI. Other heart ailments such as Coronary artery spasm which is the temporary tightening of the muscle in the artery wall can also lead to MI [1].

The risk factors for the MI include, smoking and long term exposer to second-hand smoke can damage the wall of arteries. The damage can allow deposits of cholesterol and other substances to slow down the blood flow in the coronary arteries. Smoking cause coronary artery disease and increases the risk of blood clot. Type 1 and Type 2 diabetes can increase the risk of MI. High blood pressure for a long period can damage the coronary artery. Cholesterol is the major part of deposit which can narrow the coronary artery. Obesity has

the chance of developing diabetes and high blood pressure which leads to MI. Lack of physical exercises contributes to obesity and may lead to MI.

Heart attack occurs when there is a lack of blood and oxygen flow towards the heart muscles which leads to an abnormal heart rhythm called arrhythmia which in common terms means life-threatening. Heart attack damages the heart muscle cells which in turn causes scars to appear in the heart. This condition is called myocardial ischemia in scientific terms. Long time repeated ischemia may lead to heart failure [2]. There are several medical techniques for identifying the MI. Electrocardiogram, echocardiogram, coronary angiography, Computerized Tomography (CT), Magnetic Resonance Imaging (MRI) and Positron Emission Tomography (PET) are some of them. Doctors recommend electrocardiogram for the identification of the MI. Electrodes attached on the skin record the electrical signal of the heart. Changes in the electrical signal in electrocardiogram are the sign of heart damage. Exercise can make the heart pump faster, which helps in identifying the heart problem. Stress Test, Heart rhythm, blood pressure and breathing can be measured when the patient walks on the treadmill. Echocardiogram is a process which produces images of the heart with the help of a wand-like device by analysing the continuous sound waves produced by the heart. The echocardiogram can help in identifying the area of the heart damage which is not pumping properly. Coronary Angiography, is a dye injected into the blood vessels of the heart. A series of images are taken through the x-ray machine showing the path of the dye which helps the doctor in the detailed analysis of the inner blood vessels. Whereas cardiac CT scan is to determine the calcium deposited on the walls of the artery through the images. The heart arteries can be visualized using the CT scan.

## 1.2. Medical Technologies

Medical science has advanced considerably due to the on-going technological revolution. This undoubtedly has a positive effect on MRI as well. The increase of magnetic strength in the MRI yields an easy device capability. Most installed MRI scanners come with a 1.5 model Tesla (T) magnet but the recent technology improvement includes variants such as

3.0 T and 7.0 T. The MRI works based on the strong magnetic force which aligns the nucleic spin of hydrogen atoms at very low energy state in the patient. The manipulation of the nucleic spin is done through another direction. MRI emits the radio frequency into the body of the patient. The MRI captures the energy released by the molecules of hydrogen which is transformed from high to low energy states. The energy exchange is the resonance and the resonance frequency detects the energy accordingly. The computer displays the different resonance of tissues as an image in various shades of grey. The MRI scanner normally generates 110 decibels of noise. The generated noise produced by the MRI is based on the magnetic strength. The Signal to Noise Ratio (SNR), Spatial Resolution and temporal resolution are some of the common technique used to describe the quality of the MRI.

## 1.3. Arrhythmia

The most common arrhythmia is associated with MI. Arrhythmia is a problem with the rate or rhythm of a heartbeat. Arrhythmia causes the heart to beat either too fast or too slow or irregularly. When the heartbeat is too fast, it’s called tachycardia. On the other hand when it is too slow it is called bradycardia. Arrhythmia caused by the changes in the heart tissue and the electrical activities which control the heartbeat and damages the heart. The most common test to diagnose the arrhythmia is through electrocardiogram. Causes of arrhythmia lead to changes in heart anatomy, reduced blood flow to the heart which damages the heart's electrical signal, stiffening of the heart muscle, known as fibrosis or scarring [3].

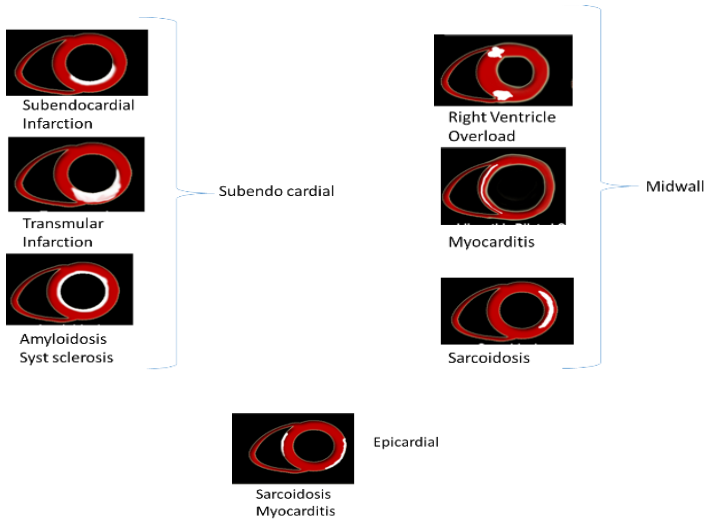


**Fig 1: Delayed enhancement of myocardial ischemia**

Fig. 1 shows the delayed enhancement of myocardial tissue. Delayed enhancement is an imaging technique for the diagnosis of various diseases including myocardial ischemia. The clinical use of the delayed enhancement of myocardial tissue is commonly performed for the evaluation of risk in the MI patient. Ischemia cardiomyopathy, is the condition of a weak heart muscle after a heart attack which is used to further examine the scar in the heart. The computer-aided machine is used to identify the ischemia cardiomyopathy within a short period of time.

Generally, the medical techniques are used by the radiologist to visually identify the scarred region in the myocardial infarcted patient [4]. The scar's length is calculated by the medical experts based on the visual identification for the prediction of arrhythmia. The main aim of the research is to identify and classify the scarred region in the heart using myocardial infarcted MRI dataset for the prediction of arrhythmia patient. The scar's volume in MI is automatically calculated for the early prognosis of high-risk arrhythmia patient for fixing the Implantable Cardioverter-Defibrillator (ICD).

## 1.4. Research Progress Summary

- Cardiac disease has become one of the leading causes of mortality in India. Ischemic heart disease and stroke are the predominant causes which are responsible for more than 80% of deaths.

- World Health Organization (WHO) survey says that the years of life lost because of heart disease increased from 23.2 million in1990 to 37 million in 2010. In the Western population, only 23% of death occurs based on heart disease before the age of 70 years and the number has increased to 52% in India.
- WHO has estimated the current burden of heart disease; India would lose $237 billion from the loss of productivity and spending it on health care over ten year period (2005-2015).

## 1.5. Research Findings

The proper assessment of the physiological impact of coronary artery stenosis on the Left Ventricle (LV) myocardium can affect the prognosis and treatment decision. Cardiac MRI captures the myocardial perfusion by imaging the myocardium during the first pass of the gadolinium with spatial and temporal resolution. The approach has been validated and verified experimentally for the early diagnosis of arrhythmia. A retrospective study was conducted using 150 myocardial infarcted MRI, which includes myocardial ischemic and nonischemic samples. The aim of the research work is to develop a predictor model with the help of machine intelligence technique using clinical heart MRI for the prediction of arrhythmia. The work focuses on efficient segmentation and classification of scar tissues in the myocardial infarcted patient's heart using magnetic resonance imaging for the computer-aided detection. The current research work involves five different phases which are mentioned below.

- Phase I: Preprocessing is performed using median filtering for reducing the noise in the MRI along with the segmentation using Morphological technique and Fuzzy C-Means for the identification of the scarred tissues in the myocardial infarcted magnetic resonance imaging.
- Phase II: Feature selection using grey thresholding and feature extraction using region growing technique.
- Phase III: Measure the scar volume using a flood fill algorithm.

- Phase IV: Build the classification model based on the scar volume using and decision tree.
- Phase V: Evaluate the classification model based on the scar volume using Levenberg-Marquardt Neural Network (LVNN).

The proposed research work is the hybrid model for the classification and prediction of arrhythmia based on the volume of the scar which is considered as one of the best models for the classification and prediction of arrhythmia.

### 1.6. Proposed Model

The proposed model is a hybrid model used to automate the classification and prediction of arrhythmia in the myocardial infarcted images using magnetic resonance imaging which gives a second opinion for doctors in identifying the high-risk arrhythmia patient for fixing ICD.

# 2. NEED FOR THE STUDY

1. An ICD is needed only when there is an electrical stimulation becomes chaotic and starts randomly in the ventricles instead of the Sinoatrial (SA) node. The unnecessary placing of the ICD may cause bleeding, damage to the vessel, infection of the incision, etc.
2. Early prediction of heart arrhythmia using MRI images is needed.
3. To use a machine intelligence with clinical heart data, which identifies the scar tissues in the heart to predict heart arrhythmia and the result is being validated using the ECG report.
4. The proposed model act as the secondary tool for the doctors to predict whether the cardiac patient needs the ICD.

# 3. RELATED WORK

Image enhancement primarily focuses to smooth the image which is used for contour identification. The image enhancement technique which works well for an X-Ray image will not be suitable for an MRI. Below is the study which is based on the medical image enhancement.

Generally, the common method for the image enhancement is histogram equalization [5] which enhances the contrast of the image by the equal distribution of gray level. The method doesn't necessarily of the contrast enhancement but damages the medical images for identification and border areas. To improve the performance different generalization have been implemented [6, 7]. Combination of histogram equalization and wavelet transform had been implemented to improve the performance on the ultrasound [8] which improved the edges and the abdominal walls for real-time performance in the dynamic applications. Gamma correction [9] is another method for image enhancement. The gamma correction method dynamic range enhances and improves the images.

Morphological filtering [10] is used for sharpening the medical images. To sharpen the existing images after applying the gradient-based operator for the edges. Morphological operators increase and decrease the colors in different parts of the medical images which play a great role in processing the images. Morphological Gradient for locating the edges in the images is one of the best comparable results with classical edge detectors as Sobel and Canny [11].

Segmentation is still one of the major challenges in medical image processing because of multiple factors like noise, poor contrast, image acquisition, and intensity which is linked with the MR signal, several tissue signal in the same pixel by the image resolution. The review process based on the MRI segmentation, intensity correction and noise reduction had been published.

An investigation based on four methods: image smoothing, phantom correction, surface fitting, and homomorphic filtering had been performed in [12]. Six retrospective method

like low-pass filtering, histogram-based, Fourier domain, model-based methods had been quantitatively and qualitatively investigated in [13]. A review based on the model-based method like hypersurface, low frequency and statistical model had been categorized in [14]. Retrospective methods which are divided into the transformed domain and grayscale based on surface fitting like spline and polynomial fitting. Spatial filtering which includes homomorphic filtering and low pass filtering and the statistical technique includes markov random fields and Fuzzy C-Means (FCM). In grayscale and probability density function, wavelet domain and Fourier domain are under the transform-based method in [15].

The FCM method is used often for the segmentation of the medical images [16, 17]. The improved FCM with information of local spatial with the classical clustering method [18, 19]. Through the local spatial information, the kernelization performance is improved by FCM [20, 21]. After the improved FCM the processing of the data is easily clustered. Zhang [22] had proposed the kernel technique for the calculation of the distance between cluster centers. More kernel-based classification is in [23-27]. FCM and clustering technique has been widely used by the researcher since there is no training is required [28-30].

Coupe et al., [31] had proposed optimized blockwise nonlocal means denoising filter for 3D MRI to reduce the noise uses natural redundancy of information. Liu et al., [32] had proposed nonlocal enhanced denoising filter for 3D MRI. The design of the filter considers the Rician noise in MRI. Manjon et al., [33] had proposed a nonlocal denoising technique for MRI with various noise levels. Hu et al., [34] had proposed a DCT based filter for MRI denoising. Nowak [35] had proposed a wavelet-based technique, Anand and Sahambi [36] for noise removable in MRI. Alexander et al., [37], Xue et al., [38] had proposed an integrated method for adaptive enhancement for global to local segmentation of the brain in 3D MRI where wavelet filter is used for denoising. Segmentation is done with the combination of spatial feature-based fuzzy clustering.

Otsu technique was proposed by Otsu in 1979. It is a global thresholding selection which is used for a simple and effective way [39]. Gong et al., [40] proposed a fast recursive technique which reduces the computational time. Otsu technique is one of the best

technique for real-world images which is based on the shape and the uniformity. To upgrade the medical images Goyal S. et al., [41] had proposed region growing adaptive enhancement. Oghli et al., [42] had proposed a fully automated region growing using GSmap and spatial information using ultrasound images. The seed point has been chosen based on the texture features from the run length and co-occurrence matrix. Segmentation is based on the thresholding and spatial information of pixel. The proposed method reduces the time than the manual region growing. Girdhar et al., [43] had proposed an adaptive region-based contrast enhancement technique which is based on the region growing.

Various techniques for enhancing the contrast, segmentation, classification and prediction based on the image processing are available. Finding the exact segmentation and classification technique is a challenging task for medical image processing. Another strategy for upgrading the result of the medical images is the hybrid technique which yields promising results.

# 4. PROBLEM STATEMENT

To design and develop a predictor model for heart arrhythmia using MRI.

# 5. OBJECTIVES OF THE STUDY

## 5.1. Primary Objective

The main objective is to develop a predictor model for an early prediction of heart arrhythmia using MRI of the myocardial infarcted patient.

## 5.2. Secondary Objectives

- The predictive model is also tested using the myocardial non-ischemic dataset, 2D enhanced myocardial ischemia MRI dataset with ground truth dataset.
- The result of the predictor model is validated and verified with radiologist.

# 6. METHODOLOGY

## 6.1. Preprocessing

Generally, methodology is the theoretical and mathematical analysis of techniques which is applied to specific study. The specific technical process used for the identification and for the deep analysis of study based on the information required for the research. A methodology has a set of rules, some guidelines, checklist and other various feature for the enhancement of quality based on the research.

### 6.1.1. Median Filtering

A median filtering which is a non-linear operation in the medical image processing used in the research to reduce the noise. The main objective of the median filtering is to reduce the noise in the image and safeguard the edges. Each pixel in the medical image is changed with the mean value of the pixel which surrounds it. The filter uses the smoothing technique based on the kernel value. Median filtering is normally used for the digital image processing whose output is the middle element of the sorted array of pixel values from the window [44].

A. Proposed Steps for MI using median filtering

Step 1: Placing the window over the image pixel

Step 2: Picking up every pixel of the image

Step 3: Sorting the pixel

Step 4: Pick the middle pixel

Step 5: Exchange the value of pixel using middle pixel in the 3x3 neighborhood

## 6.2. Segmentation

Segmentation is the process of automatic or semiautomatic identification used to locate boundaries in the images. The major challenges of the medical image segmentation are the

identification of the contour. The result of the segmented medical images is used for the diagnosis. Bong et al., [45] had proposed multiobjective clustering ensembles which include for the segmentation of nodule in Lung CT (Computed Tomography).

### 6.2.1. Morphological Filtering

Morphological operation includes dilation, erosion, opening, closing and gradient for shrinking and growing including remove or fill-in region boundary pixels which effects the holes within the region gets smaller [46]. Every pixel in the matrix is called structuring pixel.

### A. Dilation or Erosion Operation

Dilation and erosion are basic mathematical operation. Dilation and erosion are defined as follows

$$f \oplus h = \{(\hat{h})_x \cap f \neq \emptyset\} \quad (1)$$

Equation (1) explains the dilation and erosion, Where the parameters $\emptyset$ = empty set, $\hat{h}$ Shifts its origin to all the points, $G = f \oplus h$, at least one point of $\hat{h}$ is influenced in $f$.

If the origin of $h$ is influenced in $(f \subset f \oplus h)$

For erosion,

$$f \ominus h = \{x: (h)_x \subset f\} \quad (2)$$

Equation (2), explains the erosion operation in which if the origin of h takes value 1, then

$f \oplus h \subset f$ the erosion function reduces the size of the objects. The function increases the holes of an image which removes minute details of the image. Removing the brightest areas of an image makes the final image looks darker than the original image. The dilation images act in reverse, which increases and decreases the size of the image hole in an image. The opening operator is also equivalent to dilation and erosion.

## B. Closing and Opening Operator

$$f \cdot h = (f \oplus h) \ominus h \tag{3}$$

Equation (3) explains the closing of an image which smooth the contour of an image and fill the small gap and holes

$$f^{\circ}h = (f \oplus h) \oplus h \tag{4}$$

Equation (4) explains the opening of an image which smooth the contour of an image and eliminate the false touching, thin ridges and branches. The opening operator eliminates the weak connections between objects and small details, but the closing operator eliminates the small holes and fills the cracks.

### 6.2.2. Fuzzy C-Means

FCM is one of the known fuzzy clustering algorithms, which executes by assigning the membership of every data which corresponds to every cluster center based on the distance between the cluster centers [47]. Every membership data should be equal to one. After every iteration, the cluster center is updated based on the following equation

$$\mu_{ij} = \frac{1}{\left(\sum_{k=1}^{c}\left(\frac{d_{ij}}{d_{ix}}\right)\right)^{\left(\frac{2}{m-1}\right)}} \tag{5}$$

$$v_j = \left(\frac{\sum_{i=1}^{n}(\mu_{ij})^m x_i}{\sum_{i=1}^{n}(\mu_{ij})^m}\right) \tag{6}$$

$\forall_j = 1,2, \ldots \ldots . c$

Equation (5) and (6) explains the membership data and cluster center, where the parameters $\mu_{ij}$ = Membership $i^{th}$ data to $the\ j^{th}$ cluster center, $k$ is Iteration Step, $c$ is No. of the cluster center and $d_{ij}$ is Euclidean distance between $i^{th}$ data and $j^{th}$ cluster.

$$\text{Euclidean} = \sqrt{(x_2 - x_1)^2 + (y_2 - y_1)^2} \tag{7}$$

Equation (7) explains the Euclidean distance between clusters, where $(x_2 - x_1)$ is data (Pixel), $(y_2 - y_1)$ is a cluster, $d_{ik}$ is Euclidian distance between data $(i^{th})$ and iteration step $(k)$ and $M$ is Fuzziness index $m \in (1, \alpha)$ controls the fuzziness of membership.

$$j(u, v) = \sum_{i=1}^{n} \sum_{j=1}^{c} (\mu_{ij})^m \, || \, x_i - v_j ||^2 \quad (8)$$

Equation (8) explains the fuzziness of membership, where the variable $J$ is an Objective Function

## FCM Algorithm

Let $\mathrm{P} = \{\mathrm{p1}, \mathrm{p2}, \mathrm{p3} \ldots, \mathrm{pn}\}$ be the set of data points and $\mathrm{C} = \{\mathrm{c1}, \mathrm{c2}, \mathrm{c3} \ldots, \mathrm{cn}\}$ be the set of centers

Step 1: Select the $'C'$ center randomly

Step 2: The membership of fuzzy is calculated

Step 3: Computing the fuzzy center

Step 4: Repeat step 2 and step 3 until the minimum value occurs

$$\left|\left| U(k+1) - U(k) \right|\right| < \beta$$

Where the parameters,

'$k$' is the iteration step.

'$\beta$' is the termination criterion between [0, 1].

'$U = (\mu ij)n * c$' is the fuzzy membership matrix.

## 6.3. Feature Selection

Feature selection is the reduction in dimensionality through knowledge and discovery which allows the removable of unrequired features. Feature selection adds less transfer of data and efficient data mining. Feature selection plays one of the major role in the medical image processing which removes the unrequired features which improve the performance

of the data processing. Feature extraction includes three processes of the image which is ranking, screening and selecting. In screening, feature selection removes the unimportant and problematic predictor. Ranking sorts the parameters based on the importance and in selecting the process of feature extraction identifies the subset of features by preserving the most important features.

### 6.3.1. Gray Thresholding

Gray thresholding computes global thresholding using the otsu's method which can be used for converting an intensity image to binary image [48]. The Gray thresholding uses an otsu method which minimizes the intraclass variance of the black and white pixel.

### Algorithm for Gray Thresholding

Step 1: Compute histogram and probability of every intensity level.

Step 2: Initial class probability and initial class means are arranged.

Step 3: All possible maximum intensity thresholding

Step 4: Update $\mathfrak{q}i \; and \; \mu i$

Step 5: Compute the class variance

Step 6: Desired thresholding which corresponds to the maximum value between-class variance.

## 6.4. FEATURE EXTRACTION

Feature extraction is the transformation of the original image to the reduced number of features which includes discriminatory information. Feature extraction reduces the data dimensionality, remove redundancy, or irrelevant information which transforms in the form of appropriate classification [49]. Improves the classification performance which yields more stable representation. If the bandwidth of the input data is reduced then the improved processing speed is possible. Simply, extraction methods which are mainly based on the data reduction to obtain the scalar features.

### 6.4.1. Region Growing Algorithm

Region growing algorithm is also called as the seed fill algorithm which determines the area connected to the node in a multidimensional area. Region growing works with the premise of a pixel by pixel handling. The handling begins by initial picking of a pixel from the image which means seed point. The execution of any region-based approach only based on selecting the seed point. Seed determination is done through the geometrical properties of region chosen initially. The central pixel point of the region of the interest is the seed point [50]. Navigation and determination of the region start from center pixel which maintains the distance from the superfluous zero paddings. Besides the manual determination of the ROI should be utilized, which revolves around the most required pixels [51].

### Automatic Region Growing Algorithm

Step 1: The initial seed point is selected based on the partitioned histogram.

Step 2: A seed grows by merging the neighboring pixels.

Step 3: Stop the process

The region growing algorithm is tested on 2D MRI. The partitioned histogram finds the first seed point through the procedure of thresholding technique by calculating the maximum and minimum grey levels of an images. The image is divided into foreground and background images using the threshold value. The average mean value for the foreground and background images are calculated. The threshold value is updated based on adding the foreground and background mean value and finding the average of mean value. The seed point is identified based on the difference between the average mean value and seed pixel. A seed is grown by merging the neighboring pixel whose properties are similar.

## 6.5. CLASSIFICATION AND PREDICTION

Image classification based on the clinical study is a visible issue which aims for classifying medical images in various categories. Generally, medical image classification can be

divided into two steps. The initial step is an effective feature extraction from the image. The next step is feature building to build models which classify the image dataset. Previously, doctors use their experience professionally to extract the features for classifying the medical images in different classes, which is difficult, boring and time-consuming task. The approach is disposed to unpredictability or non-repeatable results. By considering the researches until now, image classification on medical application research has great merit. The researchers' efforts have led to a large number of published studies in this area. However, still now there are challenges to accomplish the task efficiently.

### 6.5.1. Decision Tree Algorithm

Decision Tree algorithm fits into supervised learning algorithms family. Unlike additional supervised learning algorithms, the decision tree algorithm can be used for classification problems and for solving regression too. In general, the motivation of using decision tree is for creating the training model which is used for predicting classes or values of variables which have been targeted by learning decision rules indirect to prior data i.e., trained dataset. The level of understanding towards the decision trees algorithm is easy when compared with the other algorithms based on the classification. The decision tree algorithm is to give a solution to the problem, by tree representation [52]. Every internal node of the tree which corresponds to attribute and every leaf node resembles the label of the class.

**Pseudocode for Decision Tree**

GenDecTree (Sample S, Features F)

Step 1: If stopping_condition (S, F) = true then

a. Leaf=createnode()
b. Leaf.label=classify(s)
c. Return leaf

Step 2: Root=createNode ()

Step 3: Root.test_condition=findBestSplit(S, F)

Step 4: $V = \{v | v\ a\ possible\ outcome\ of\ Root.test_condition\}$

Step 5: For each value $v \in V$

a. $s_v \coloneqq \{s \mid root.testcondition(s) = v\ and\ s \in S\}$
b. $child = GenDecTree(s_v, F)$
c. Add a child (root→ $child$) $as\ v$

Step 6: Return root

# 7. EVALUATION OF CLASSIFIER MODEL

Classification model evaluation is required to evaluate the metric for the quantification performance of the model. Classification is one of the supervised learning which deals with different categories. The training model is used to predict the unwanted labels of the data. In general, there are different types of algorithm which have different technology for the classification problem. But in the end, the most needed one is to find a suitable algorithm for the particular classification problem. There are different evaluation algorithm for predicting the suitable algorithm for the classification problem. So, in the proposed model for evaluating the classification model the research work includes the Feed Forward Neural Network (FFNN) as the referential classifier.

## 7.1. Feed Forward Neural Network

The proposed classification model is evaluated using the FFNN which is used as the referential classifier for finding the classification accuracy of the build classification model. The FFNN aims to estimate some function. The classifier maps and input value to the classifier. FFNN describes the mapping and learns the parameters which give the best result. A collection of neurons together forms a network which represents the graph-like structure. Neurons are represented by nodes, arrows represent the link of nodes. Every node has its numbers and a link which connect the two nodes has a pair of numbers. The network without the cycle is called the FFNN. Input nodes are with the variable$(x_1, x_2 \dots \dots \dots x_m)$. The variable will not compute but process the nodes by passing the value. Output nodes are with the variable $(y_1, y_2, \dots \dots \dots y_m)$. The Neural Network (NN) has hidden layers

which are connected to the inner network. By numbering the weights each $j^{th}$ node has a set of weights $w_{ij}$. A network is completely explained through the graph, the set of weight and the functions $'f'$ of every node. FFNN is also called as the Deep feed-forward network are the deep learning model.

### 7.1.1. Algorithm for Training the Supervised Learning

Step 1: First, set the weight $w_{ij}$ to random values

Step 2: Repeat the following steps

(1) Place the input value $x$ in the training set.

(2) Compute the output network $f(x)$

(3) Change the node weight $w_{ij}$ of the nodes

Step 3: Continue until the small error $c(y, f(x))$

# 8. RESULTS AND DISCUSSION

In the section, the results of myocardial ischemia dataset are presented and complete illustration of identifying the scar region in the delayed enhancement myocardial infarcted dataset is explained. The term sudden cardiac death risk assessment is named as Intelligent Analytical Arrhythmia Predictor (IAAP) methodology. The results demonstrate the IAAP significant outperforms in clinical proof and early predicts the arrhythmia. In a proof of concept study, the IAAP is compared with the clinical metrics.

## 8.1. Proposed Model

The proposed model includes five phases. Fig 2 depicts the flow of the proposed model based on the phases for 3D enhanced myocardial ischemia MRI which is named as IAAP.

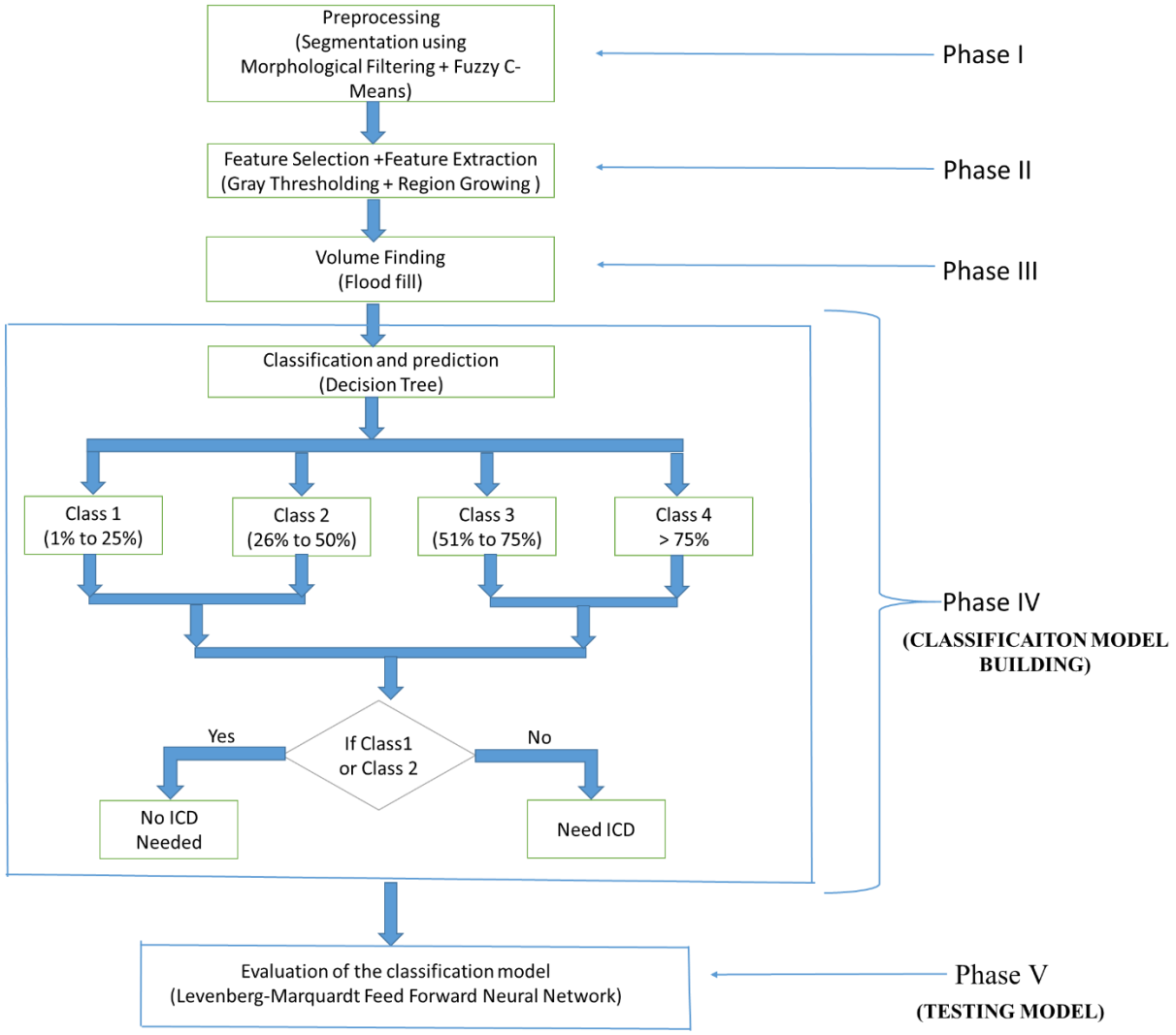


**Fig 2: Model for IAAP approach**

Phase I, delayed enhancement myocardial infarcted dataset is preprocessed using the median filtering and compared with the Gaussian blur, contrast enhancement, mean filtering along with morphological filtering and FCM for segmentation. Phase II, Gray thresholding and region growing are assigned for the feature selection and feature extraction, the phase II stage is important for identifying and extracting the scar region. Phase III, volume finding using the flood fill algorithm. Volume finding can't be currently acquired in the clinical MRI, they are calculated visually therefore, the estimation of the volume of scar region is one of the novel work included in the proposed model. The next phase IV is to classify and predict whether the scar volume leads to early prediction of

arrhythmia using and decision tree. The proposed model concludes that the patient will not lead to arrhythmia, if the scar volume falls under class 1 and class 2. Similarly, the proposed model also concludes that the patient will lead to arrhythmia if the scar volume falls under class 3 and class 4. Finally, in phase V the proposed classification model is evaluated based on FFNN classifier with the help of scar volume. The result of the proposed model is also validated with the medical expert.

## 8.2. The Predictive Capability of IAAP

The predictive capability of the IAAP approach was evaluated based on the 150 patients with delayed enhancement with 110 training and 40 testing. The IAAP approach is compared with the processing of clinical manual. The compared result reveals that the IAAP is one of the significant models for the early risk finding of arrhythmia. The results has been validated by clinical experts and stated that the results are accurately predicting arrhythmia patient.

### 8.2.1. Dataset Description

The dataset includes 150 myocardial infarcted two dimensional MRI. The size of the images in the dataset includes 8-bit intensity images and 16-bit intensity images. The dataset has been retrieved from a cardiac atlas which includes a prospective, multicenter, randomized clinical trial with coronary artery diseases and left ventricle dysfunction. The primary objective of the study is to test the hypothesis that Implantable Cardioverter Defibrillator (ICD) therapy in combination with medical therapy, in patients with myocardial infarct. The secondary endpoint is a survival from mortality due to the onset of fatal cardiac rhythm disturbances. The dataset includes the various resolution depending on heart rate and breath-hold duration. Short-axis slices are acquired to cover the whole heart. Late gadolinium enhancement imaging are performed using segmented spoiled gradient recalled echo imaging with an inversion recovery magnetization preparation, 10 to 20 minutes after intravenous injection of a gadolinium-based contrast agent (0.15 to 0.2

mMol/kg body weight). Delayed enhancement images are also acquired in the same planes and image-slice positions [53].

### 8.2.2. Phase I

Before the MI of MRI data, enter into the proposed model the first stage is to identify the noise in the MRI. In general, the MRI has been affected by the noise based on MR field strength. The dataset of MI patients has been taken in 1.5 T field strength and the manufacturer is GE medical system. The noises which affect the MRI are gaussian noise, speckle noise, salt and pepper noise and poisson noise. Based on the histogram shape it has been identified that the dataset is affected with the speckle noise. The noise is calculated based on the signal to noise ratio (SNR).

Fig 3 shows the histogram image shape of patient 1 before the noise removal.

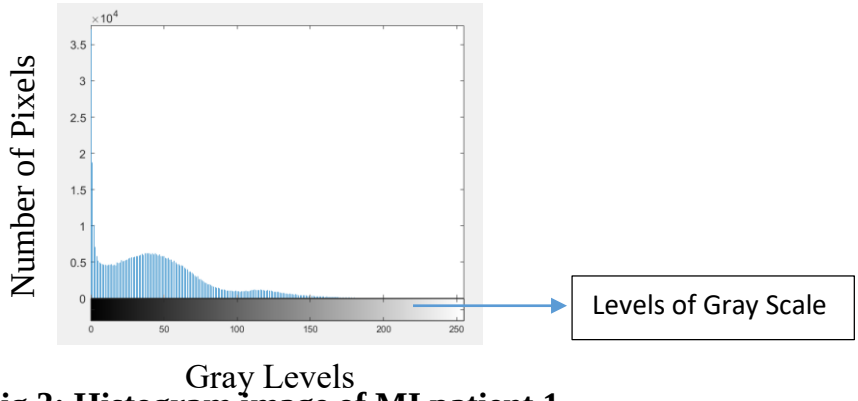


**Fig 3: Histogram image of MI patient 1**

Fig 4 shows the histogram image shape of patient 2 before the noise removal.

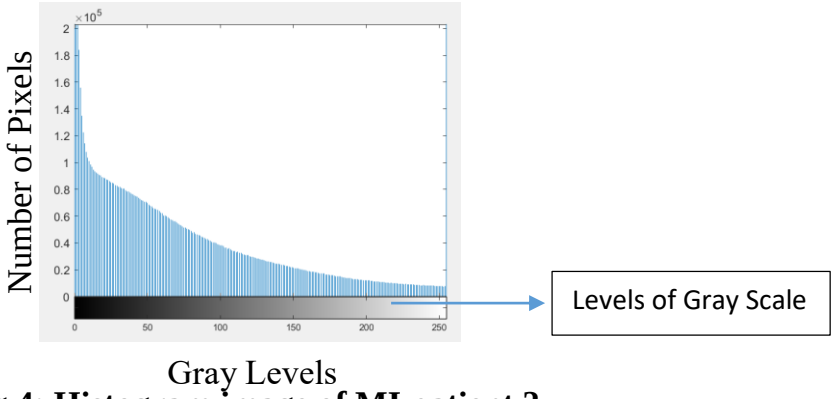


**Fig 4: Histogram image of MI patient 2**

Fig 5 shows the histogram image shape of patient 3 before the noise removal.

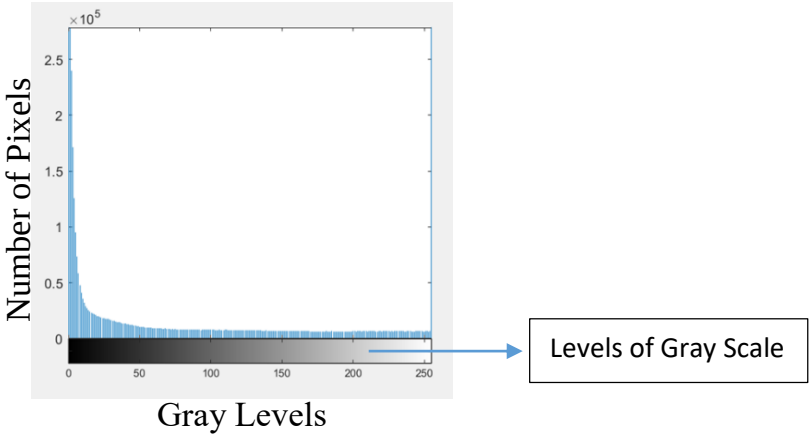


**Fig 5: Histogram image of MI patient 3**

The shape of the histogram for patient 1, patient 2 and patient 3 specifies the speckle noise. To reduce the noise in the MI of MRI the median filtering technique which works well in removing the speckle noise has been identified through literature review and applied to the dataset and below is the result based on the MRI images.

**Table 1: Preprocessing using median filtering (Phase I)**

| S.NO | Original image | Median Filter |
|---|---|---|
| 1. | 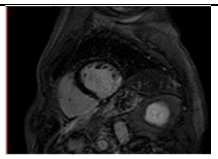 | 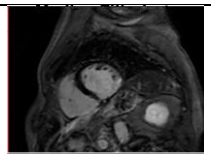 |
| 2. | 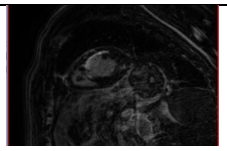 | 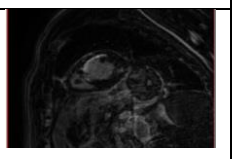 |
| 3. | 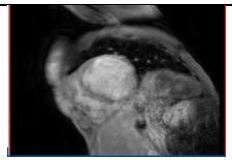 | 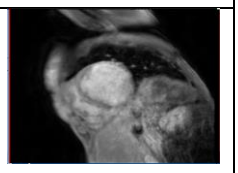 |

Table 1 shows the results of 3 patients with various sizes of scar volume and scar occurrence in a different position. The median filtering reduces the noise in the delayed enhancement myocardial infarcted MRI. Sample 1, 2 and 3 are the 3 samples with delayed enhancement myocardial infarction and the noise reduction image. To evaluate the result

of the median filtering of the delayed enhancement myocardial infarction is compared with gaussian blur, bilateral filter and mean filtering. The result reveals the median filtering reduces the noise and protects the edges. Table 2 illustrated the comparative results of the gaussian blur, bilateral filter and mean filtering based on the median filtering.

**Table 2: Performance Evaluation on various filtering technique**

| S. No. | Original Image | Gaussian Blur | Bilateral Filtering | Mean Filtering |
|---|---|---|---|---|
| 1. | 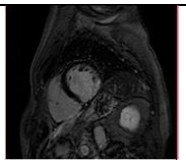 | 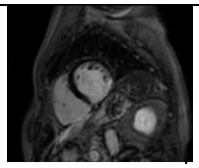 | 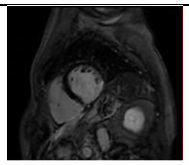 | 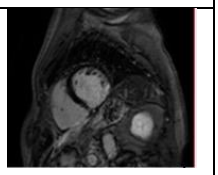 |
| 2. | 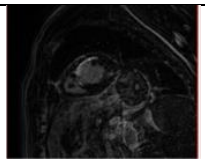 | 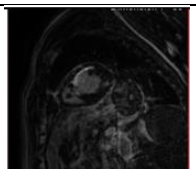 | 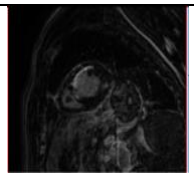 | 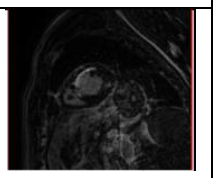 |
| 3. | 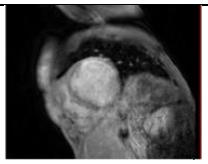 | 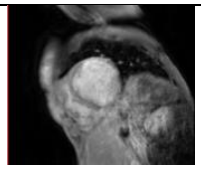 | 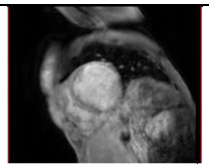 | 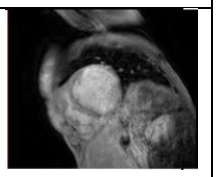 |

The comparative results reveal that the median filtering had significantly given better results than the Gaussian blur, bilateral filtering and mean filtering. Median filtering results also provides the enhancement effect. After applying the median filtering the images are evaluated using the histogram again to check whether the speckle noise in the image has been reduced and also verified using SNR value.

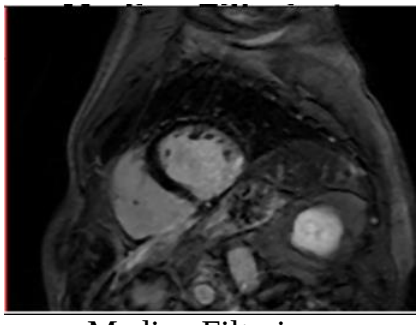

Median Filtering

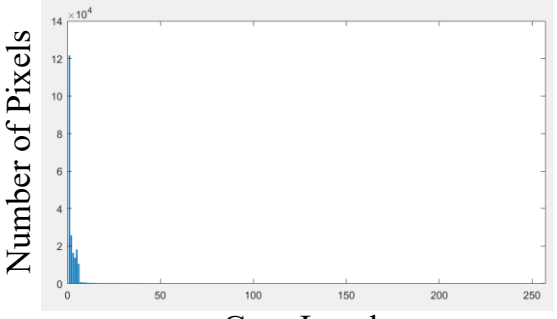


**Fig 6: Histogram image after noise removal (Patient 1)**

Fig 6 depicts the histogram image of patient 1 after the removal of speckle noise and the SNR value is 21.65. This show that the quality of the image is acceptable to proceed for the next level.

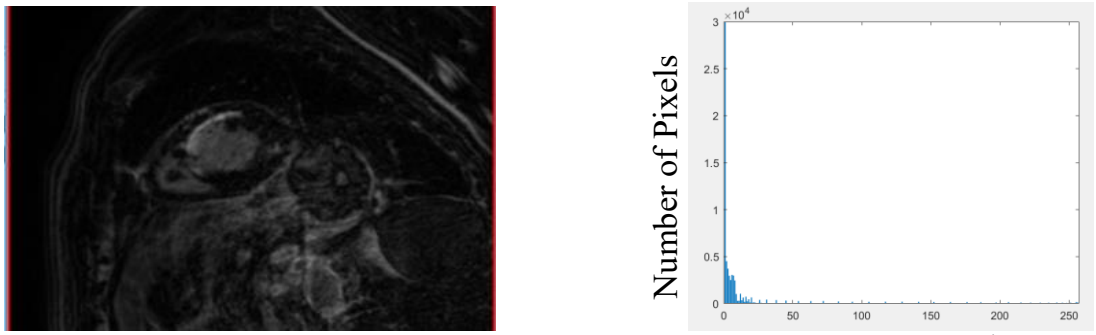


**Fig 7: Histogram image after noise removal (Patient 2)**

Fig 7 depicts the histogram image of patient 2 after the removal of speckle noise and the SNR value is 21.65. This show that the quality of the image is acceptable to proceed for the next level.

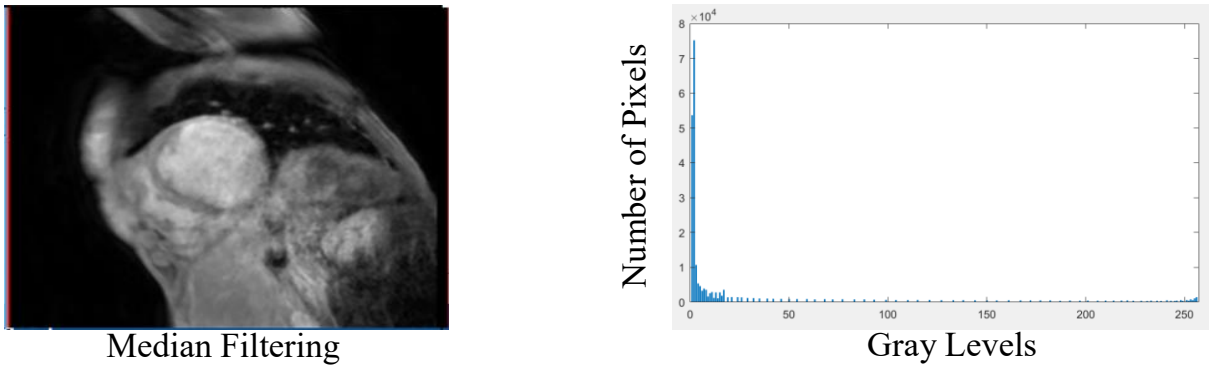


**Fig 8: Histogram image after noise removal (Patient 3)**

Fig 8 depicts the histogram image of patient 3 after the removal of speckle noise and the SNR value is 21.65. This show that the quality of the image is acceptable to proceed for the next level. Table 3 represents the segmentation technique of morphological filtering.

**Table 3: Segmentation based on a morphological filtering technique**

| S.NO | Median Filtering | Morphological Filtering |
|---|---|---|
| 1. | 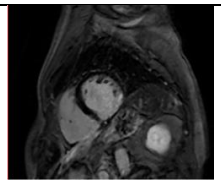 | 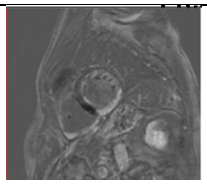 |
| 2. | 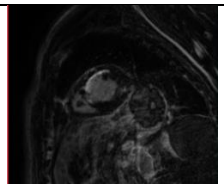 | 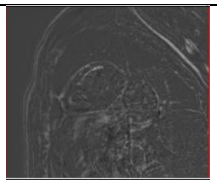 |
| 3. | 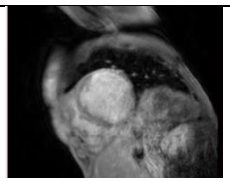 | 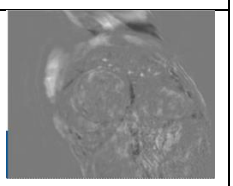 |

**Table 4: Comparative results of preprocessing algorithm**

| S.NO | Original Image | Gaussian Blur | Bilateral Filter | Mean Filtering | Median + Morphological Filtering |
|---|---|---|---|---|---|
| **1.** | 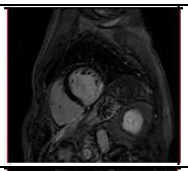 | 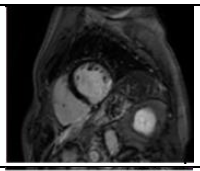 | 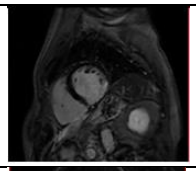 | 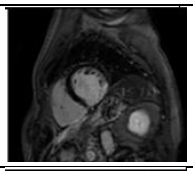 | 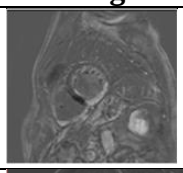 |
| **2.** | 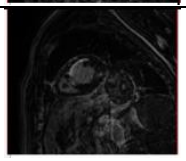 | 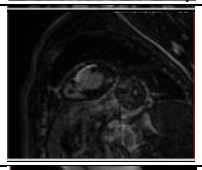 | 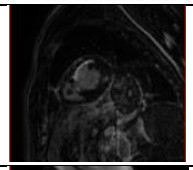 | 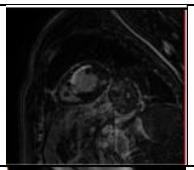 | 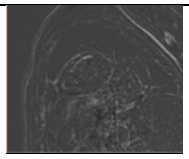 |
| **3.** | 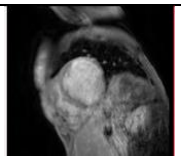 | 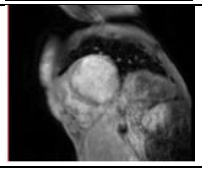 | 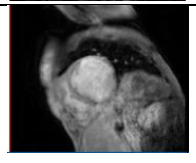 | 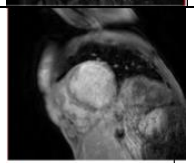 | 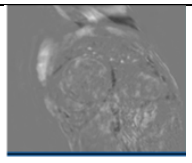 |

Table 4 illustrates the comparative results of preprocessing algorithm with median and morphological technique. The result shows that the median and morphological filtering technique enhances the images and identifies the scar region on the delayed enhancement myocardial infarction MRI.

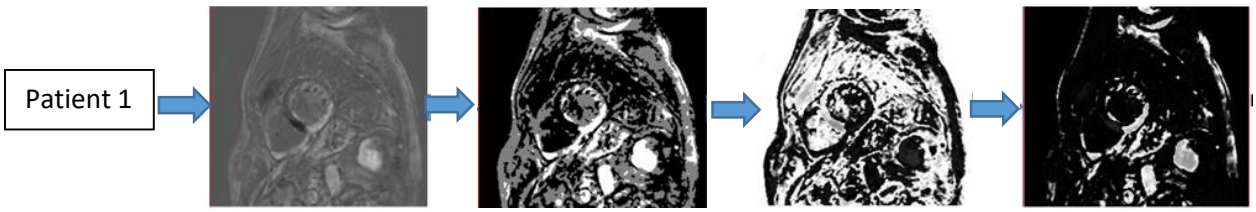


**(a) (b) (c) (d)**

**Fig 9: Segmentation using FCM for patient 1**

Fig 9 shows the segmentation of FCM for patient 1, 9(a) is the median filtering and morphological filtering, 9(b), 9(c) and 9(d) shows the segmentation results of FCM.

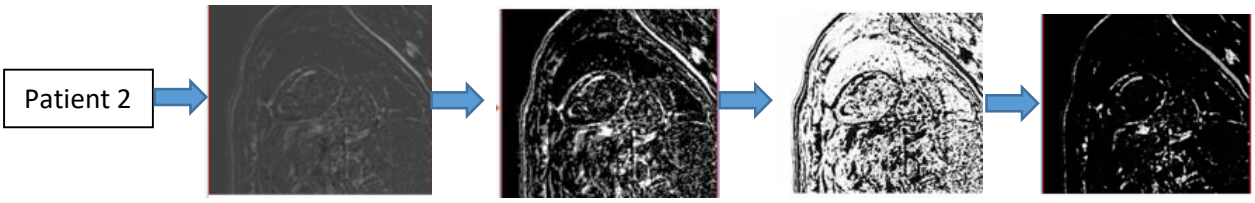


**(a) (b) (c) (d)**

**Fig 10: Segmentation using FCM for patient 2**

Fig 10 shows the segmentation of FCM for patient 2, 10(a) is the median filtering and morphological filtering, 10(b), 10(c) and 10(d) shows the segmentation results of FCM.

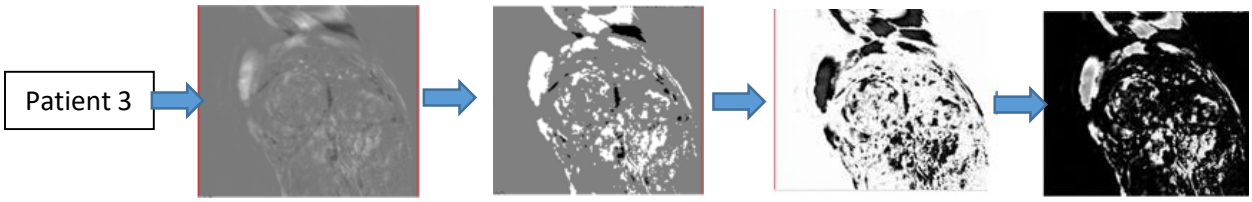


**Fig 11: Segmentation using FCM for patient 3**

Fig 11 shows the segmentation of FCM for patient 3, 11(a) is the median filtering and morphological filtering, 11(b), 11(c) and 11(d) shows the segmentation results of FCM.

**Table 5: Comparative results of segmentation algorithms**

| S.NO | Original Image | FCM | Edge Detection | Histogram Equalization | Morphological Gradient | Efficient Watershed |
|---|---|---|---|---|---|---|
| 1. | 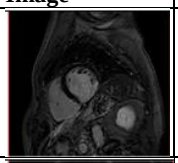 | 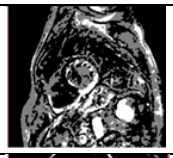 | | | 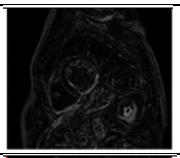 | 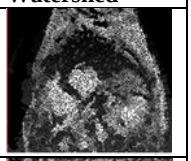 |
| 2. | 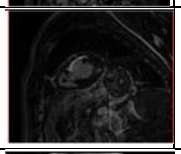 | 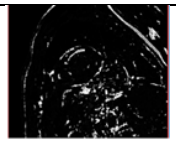 | 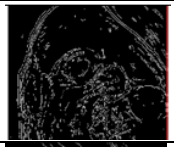 | 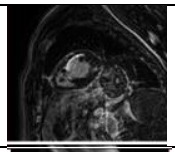 | 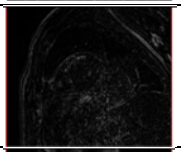 | 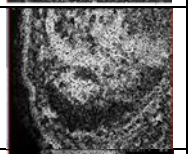 |
| 3. | 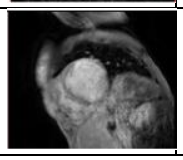 | 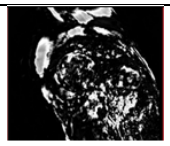 | | 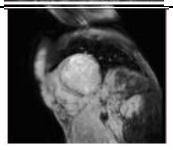 | 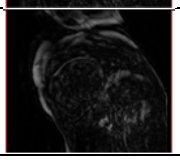 | 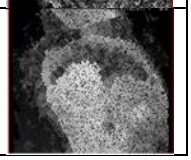 |

Table 5 shows the comparative results of segmentation algorithms. Phase II includes the feature selection using the gray thresholding and feature extraction using the otsu technique.

## 8.2.3. Phase II

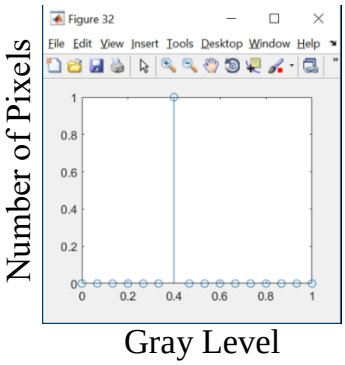


**Fig 12: Feature selection using gray thresholding (patient 1)**

Fig 12 shows the feature selection using the gray thresholding which gives the single threshold value is 0.4 for patient 1 which separates the foreground and background.

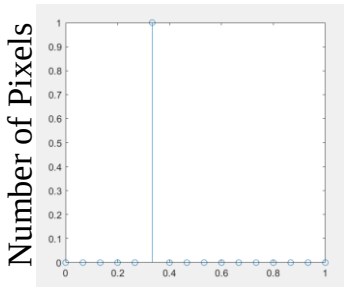


**Fig 13: Feature selection using gray thresholding (patient 2)**

Fig 13 shows the feature selection using the gray thresholding which gives the single threshold value is 0.3 for patient 1 which separates the foreground and background.

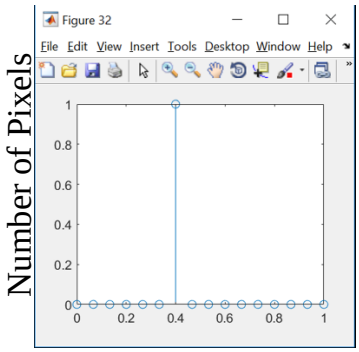


**Fig 14: Feature selection using gray thresholding (patient 3)**

Fig 14 shows the feature selection using the gray thresholding which gives the single threshold value is 0.4 for patient 1 which separates the foreground and background.

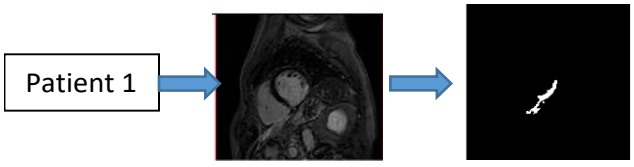


(a) (b)

**Fig 15: Feature extraction using region growing (patient 1)**

Fig 15 shows the result of feature extraction using region growing technique in MI patient after the feature selection based on the threshold value, fig 15(a) shows the original image and fig 15(b) shows the extracted scar of patient 1.

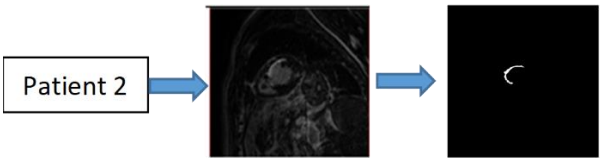


(a) (b)

**Fig 16: Feature extraction using region growing (patient 2)**

Fig 16 shows the result of feature extraction using region growing technique in MI patient after the feature selection based on the threshold value, fig 16(a) shows the original image and fig 16(b) shows the extracted scar of patient 2.

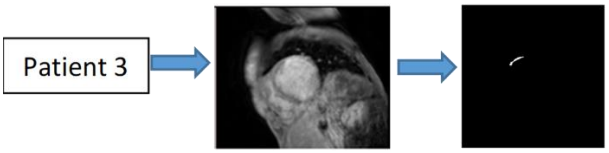


(a) (b)

**Fig 17: Feature extraction using region growing (patient 3)**

Fig 17 shows the result of feature extraction using region growing technique in MI patient after the feature selection based on the threshold value, Fig 17(a) shows the original image and Fig 17(b) shows the extracted scar of patient 3.

### 8.2.4. Phase III

After the features have been extracted from the MI patients the volume is calculated based on the flood fill algorithm with the bounding box which includes the height, width and the depth of the image. The scar volume for patient 1 is 62.4. The scar volume for the patient 2 is 78.3 and the scar volume for the patient 3 is 35.1. Based on the volume of the scar the patient will be classified and predicted.

### 8.2.5. Phase IV

Phase IV includes the classification and prediction based on decision tree which includes four classes. The patient is classified based on the classes. Class 1 is 1% to 25%, class 2 is

26% to 50%, class 3 is 51% to 75% and finally class 4 is above 75%. If the patient falls under class 1 and class 2, then the prediction states that the patient doesn't require ICD (Implantable Cardioverter Defibrillator). If the patient falls under class 3, then the prediction states that the patient requires ICD. Finally, if the patient falls under class 4, then the prediction states there is no treatment required. Fig 18 shows the comparative results of proposed scar volume classification with ground truth image of medical expert's. Based on the volume measure the prediction result shows that the patient1 require ICD.

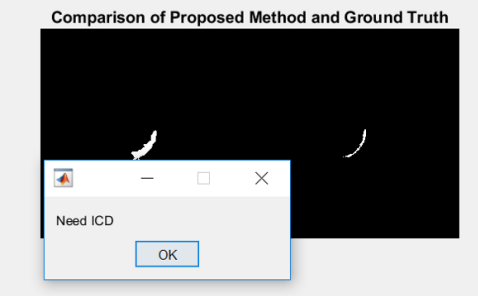


**Fig 18: Prediction based on the scar volume (Patient 1)**

Fig 19 shows the comparative results of proposed scar volume classification with ground truth image of medical expert's. Based on the volume measure the prediction result shows that the patient2 require ICD.

**Fig 19: Prediction based on the scar volume (Patient 2)**

Fig 20 shows the comparative results of proposed scar volume classification with ground truth image of medical expert's. Based on the volume measure the prediction result shows that the patient3 require ICD.

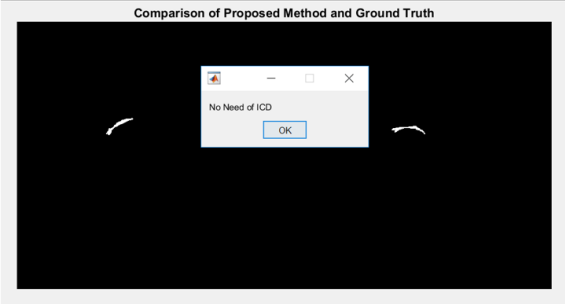


**Fig 20: Prediction based on the scar volume (Patient 3)**

### 8.2.6. Phase V

Phase V includes the evaluation process based on the classification of scar volume retrieved though the proposed model and with the medical expert's results using FFNN. The FFNN is used as the referential classifier to know the classification performance of the proposed classifier model. The result based on the referential classifier reveals that the proposed model yields 99.5% accuracy.

### 8.2.7. Matrix Evaluation

The digital grayscale image is presented in the system using the pixel matrix. Every pixel of an image is viewed by the matrix element and the integer value represented as 0 to 255. The numerical values are changed from zero (black pixels) to 255 represents the white pixels. Each image processing technique is processed through the matrix and observed on the image matrix. The proposed model is also evaluated based on the matrix and the results are as follows.

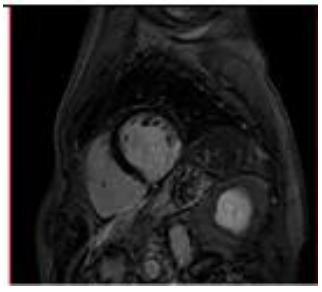

(a)

| | | | | | | | | | | |
|---|---|---|---|---|---|---|---|---|---|---|
| 41 | 29 | 18 | 49 | 62 | 57 | 58 | 49 | 26 | 11 | |
| 41 | 27 | 13 | 29 | 44 | 41 | 31 | 19 | 8 | 7 | |
| 42 | 25 | 13 | 17 | 33 | 36 | 18 | 0 | 0 | 7 | |
| 41 | 36 | 34 | 32 | 27 | 17 | 0 | 0 | 6 | 8 | |
| 38 | 41 | 48 | 43 | 18 | 0 | 0 | 0 | 5 | 0 | |
| 36 | 35 | 37 | 33 | 20 | 10 | 15 | 13 | 6 | 2 | |
| 38 | 37 | 34 | 32 | 24 | 18 | 16 | 12 | 10 | 8 | |
| 40 | 42 | 35 | 22 | 11 | 13 | 10 | 1 | 0 | 2 | |
| 38 | 34 | 21 | 13 | 17 | 19 | 9 | 4 | 7 | 7 | |
| 33 | 24 | 22 | 26 | 20 | 9 | 6 | 9 | 12 | 8 | |
| 34 | 33 | 35 | 19 | 4 | 7 | 6 | 2 | 0 | 1 | |
| 50 | 44 | 20 | 0 | 4 | 9 | 5 | 3 | 2 | 2 | |
| 59 | 33 | 0 | 0 | 4 | 0 | 3 | 7 | 4 | 2 | |
| 45 | 11 | 0 | 6 | 2 | 0 | 3 | 3 | 3 | 4 | |
| 23 | 0 | 3 | 5 | 3 | 4 | 5 | 4 | 7 | 8 | |
| 8 | 0 | 6 | 4 | 2 | 4 | 6 | 6 | 3 | 0 | |
| 0 | 0 | 8 | 8 | 9 | 10 | 7 | 4 | 5 | 6 | |

(b)

**Fig 21: Matrix value of an MRI (Patient 1)**

Fig 21 represents the original image in (a) and the matrix value which is the pixel intensity of an image in patient 1.

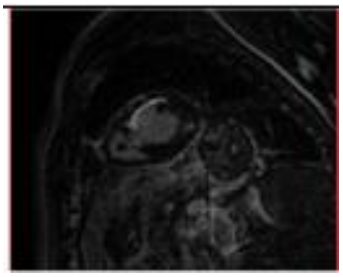

| | | | | | | | | | | | | |
|---|---|---|---|---|---|---|---|---|---|---|---|---|
| 63 | 41 | 22 | 5 | 9 | 23 | 36 | 45 | 50 | 53 | 53 | 45 | |
| 73 | 54 | 33 | 24 | 26 | 21 | 20 | 33 | 49 | 55 | 49 | 34 | |
| 71 | 55 | 39 | 34 | 37 | 31 | 16 | 23 | 42 | 48 | 37 | 21 | |
| 55 | 41 | 31 | 26 | 30 | 33 | 26 | 22 | 33 | 38 | 30 | 17 | |
| 31 | 20 | 17 | 17 | 20 | 28 | 34 | 35 | 36 | 36 | 32 | 23 | |
| 15 | 11 | 16 | 21 | 17 | 23 | 39 | 48 | 49 | 43 | 36 | 28 | |
| 19 | 20 | 29 | 30 | 15 | 25 | 48 | 56 | 55 | 46 | 36 | 29 | |
| 41 | 47 | 50 | 36 | 9 | 30 | 52 | 58 | 54 | 43 | 32 | 24 | |
| 67 | 74 | 64 | 36 | 5 | 29 | 46 | 51 | 47 | 38 | 27 | 17 | |
| 77 | 84 | 67 | 35 | 12 | 30 | 43 | 45 | 41 | 34 | 23 | 13 | |
| 71 | 81 | 62 | 32 | 29 | 40 | 44 | 42 | 38 | 30 | 19 | 10 | |
| 61 | 68 | 48 | 32 | 40 | 40 | 34 | 31 | 31 | 24 | 14 | 7 | |
| 48 | 43 | 33 | 34 | 38 | 30 | 21 | 21 | 22 | 18 | 12 | 8 | |
| 34 | 21 | 25 | 32 | 29 | 21 | 21 | 23 | 21 | 18 | 14 | 10 | |
| 26 | 15 | 22 | 30 | 25 | 18 | 24 | 28 | 26 | 22 | 17 | 10 | |
| 23 | 18 | 24 | 28 | 23 | 17 | 23 | 29 | 29 | 25 | 18 | 9 | |
| 24 | 27 | 22 | 21 | 21 | 16 | 16 | 20 | 23 | 22 | 16 | 8 | |

**(a)** **(b)**

**Fig 22: Matrix value of an MRI (Patient 2)**

Fig 22 represents the original image in (a) and the matrix value which is the pixel intensity of an image in patient 2.

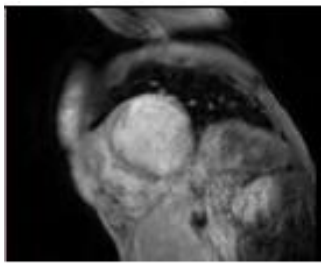

| | | | | | | | | | | | | |
|---|---|---|---|---|---|---|---|---|---|---|---|---|
| 9 | 24 | 33 | 34 | 27 | 16 | 6 | 1 | 1 | 2 | 4 | | |
| 8 | 13 | 29 | 37 | 34 | 24 | 12 | 3 | 0 | 1 | 4 | | |
| 30 | 5 | 20 | 35 | 39 | 32 | 20 | 8 | 1 | 1 | 3 | | |
| 54 | 26 | 10 | 29 | 40 | 38 | 28 | 16 | 6 | 1 | 2 | | |
| 78 | 49 | 21 | 21 | 36 | 40 | 35 | 25 | 13 | 5 | 2 | | |
| 100 | 73 | 41 | 18 | 27 | 39 | 40 | 33 | 21 | 10 | 3 | | |
| 121 | 96 | 65 | 31 | 17 | 33 | 42 | 39 | 30 | 18 | 8 | | |
| 142 | 119 | 90 | 54 | 21 | 25 | 40 | 44 | 37 | 26 | 14 | | |
| 165 | 143 | 115 | 79 | 40 | 20 | 35 | 45 | 44 | 34 | 22 | | |
| 186 | 166 | 140 | 104 | 63 | 28 | 28 | 43 | 48 | 41 | 30 | | |
| 204 | 186 | 161 | 126 | 85 | 44 | 22 | 37 | 48 | 47 | 37 | | |
| 217 | 201 | 177 | 145 | 106 | 63 | 28 | 28 | 44 | 49 | 44 | | |
| 229 | 212 | 190 | 161 | 126 | 85 | 45 | 23 | 37 | 48 | 48 | | |
| 242 | 224 | 202 | 176 | 145 | 108 | 67 | 33 | 29 | 44 | 49 | | |
| 255 | 238 | 217 | 193 | 163 | 128 | 89 | 49 | 25 | 36 | 47 | | |
| 255 | 255 | 236 | 210 | 180 | 146 | 107 | 66 | 31 | 25 | 40 | | |
| 255 | 255 | 255 | 228 | 196 | 160 | 122 | 83 | 45 | 19 | 28 | | |

**(a)** **(b)**

**Fig 23: Matrix value of an MRI (Patient 3)**

Fig 23 represents the original image in (a) and the matrix value which is the pixel intensity of an image in patient 3.

### 8.2.7.1. Median Filtering in Matrix Format

**Table 6: Median Filtering Matrix value**

| Patient 1 | Patient 2 | Patient 3 |
|---|---|---|
| 15 32 30 49 58 49 3 21 22 14 1<br>34 32 30 46 58 53 22 19 20 7 1<br>34 40 30 46 33 53 33 19 20 7 5<br>26 44 30 48 33 29 33 27 16 7 5<br>18 44 36 48 45 29 31 27 16 7 3<br>17 57 36 42 56 31 31 25 0 4 3<br>17 57 33 28 56 35 30 19 0 4 5<br>53 49 33 28 36 35 24 15 0 9 6<br>60 49 38 55 36 26 24 14 2 9 6<br>60 51 38 62 40 26 24 8 3 1 2<br>60 51 32 62 50 23 23 6 4 1 1<br>40 50 32 51 50 23 23 1 7 7 0<br>27 50 55 51 45 23 23 1 6 8 0<br>27 50 55 51 39 24 6 1 6 8 6<br>39 47 56 53 39 24 6 3 3 6 6<br>49 45 56 53 45 28 2 3 2 2 5 | 79 25 49 38 31 71 51 25 45<br>78 23 49 33 30 71 51 25 34<br>61 22 50 27 29 69 51 30 21<br>39 22 50 24 17 60 54 43 21<br>25 22 45 24 16 49 58 68 23<br>25 21 24 21 16 46 62 68 28<br>48 21 24 16 19 46 65 62 28<br>48 23 66 16 26 49 67 62 24<br>35 24 99 16 34 49 67 74 17<br>15 24 129 16 38 38 62 76 13<br>15 17 165 14 48 27 62 76 10<br>48 16 205 14 63 27 61 69 8<br>64 16 233 32 72 42 61 64 8<br>64 22 233 32 72 42 50 59 10<br>44 24 217 22 61 36 37 59 10<br>39 26 195 20 55 31 24 68 9<br>39 26 184 15 55 31 24 68 8 | 1 0 0 5 178 94 76<br>1 0 0 6 182 94 69<br>1 0 0 8 186 94 69<br>0 0 2 9 194 95 70<br>0 0 3 10 205 97 70<br>0 1 4 11 215 100 70<br>0 1 5 12 221 100 67<br>1 1 5 12 223 95 67<br>1 1 3 11 223 83 72<br>1 0 2 10 222 71 78<br>0 0 2 10 221 63 81<br>0 0 2 8 216 63 81<br>0 0 2 5 209 67 81<br>1 0 2 3 201 73 85<br>1 1 3 3 194 74 91<br>0 1 3 4 188 74 93<br>0 2 3 4 181 73 93 |

Table 6 shows the patient 1, patient 2 and patient 3 matrix value after the median filtering.

### 8.2.7.2. Region Growing in Matrix Format

Table 7 depicts the region growing value after the segmentation and feature selection.

**Table 7: Region Growing Matrix value**

| Patient 1 | Patient 2 | Patient 3 |
|---|---|---|
| 1 1 1 1 1 1 1 1 1 1 1<br>1 1 1 1 1 1 1 1 1 1 1<br>1 1 1 1 1 1 1 1 1 1 1<br>1 1 1 1 1 1 1 1 1 1 1<br>0 1 1 1 1 1 1 1 1 1 1<br>0 0 1 1 1 1 1 1 1 1 1<br>0 0 0 1 1 1 1 1 1 1 1<br>0 0 0 0 1 1 1 1 1 1 1<br>0 0 0 0 0 1 1 1 1 1 1<br>1 0 0 0 0 0 1 1 1 1 1<br>1 1 0 0 0 0 0 1 1 1 1<br>1 1 0 0 0 0 0 0 1 1 1<br>1 1 1 0 0 0 0 0 1 1 1<br>1 1 1 0 0 0 0 0 0 0 1<br>1 1 1 1 0 0 0 0 0 1 1<br>1 1 1 1 1 0 0 0 1 1 1<br>1 1 1 1 1 0 0 1 1 1 1 | 1 1 1 1 1 1 1 1 1 1 1<br>1 1 1 1 1 1 1 1 1 1 1<br>1 1 1 1 1 1 1 1 1 1 1<br>1 1 1 1 1 1 1 1 1 1 1<br>0 1 1 1 1 1 1 1 1 1 1<br>1 1 1 1 1 1 1 1 1 1 1<br>1 1 1 1 1 1 1 1 1 1 1<br>1 0 0 1 1 1 1 1 1 1 1<br>1 0 0 0 1 1 1 1 1 1 1<br>1 0 0 0 0 1 1 1 1 1 1<br>1 1 0 0 0 0 1 1 1 1 1<br>1 1 1 0 0 0 0 1 1 1 1<br>1 1 1 1 0 0 0 0 1 1 1<br>1 1 1 1 1 0 0 0 1 1 1<br>1 1 1 1 1 1 1 1 1 1 1 | 1 1 1 1 1 1 1 1 1 1 1<br>1 1 1 1 1 1 1 1 1 1 1<br>1 1 1 0 0 0 0 1 1 1 1<br>1 1 0 0 0 0 0 1 1 1 1<br>1 1 0 0 0 0 0 1 1 1 1<br>1 1 1 0 0 0 0 1 1 1 1<br>1 1 1 1 0 1 1 1 1 1 1<br>1 1 1 1 1 1 1 1 1 1 1<br>1 1 1 1 1 1 1 1 1 1 1<br>1 1 1 1 1 1 1 1 1 1 1<br>1 1 1 1 1 1 1 1 1 1 1<br>1 1 1 1 1 1 1 1 1 1 1<br>1 1 1 1 1 1 1 1 1 1 1<br>1 1 1 1 1 1 1 1 1 1 1<br>1 1 1 1 1 1 1 1 1 1 1 |

The pixel value ‘1’ represent class 1 and the pixel value ‘0’ represent class 2 which is the extracted region of scar of the MI patient.

### 8.2.8. Experiment Evaluation on Proposed Model Using Normal Heart

The proposed model is investigated based on various aspects. This section focus on implementing proposed model using normal heart.

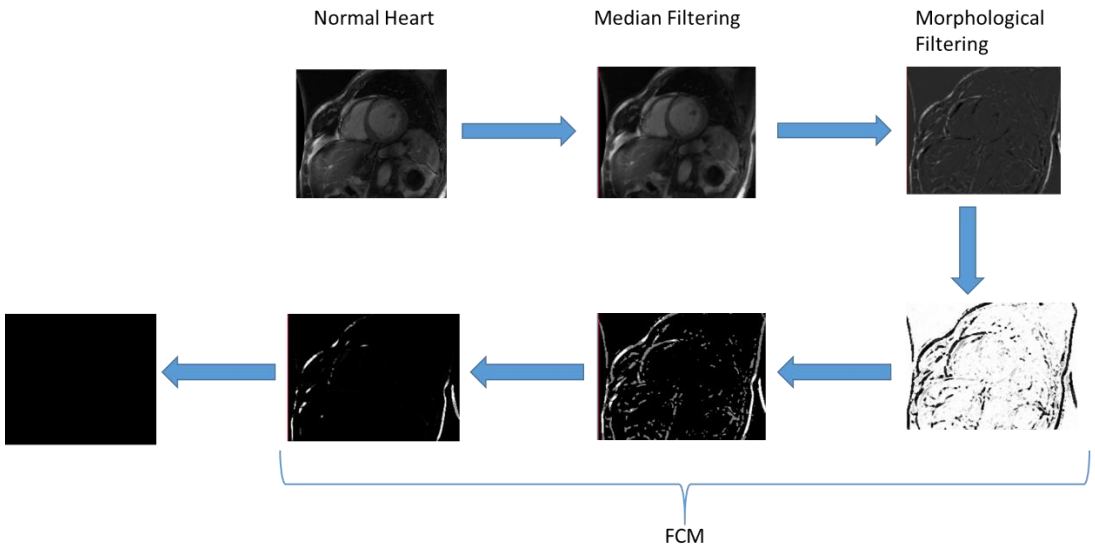


**Fig 24: Normal heart process through proposed model**

Fig 24 depicts the process of normal heart based on the proposed model. The main aim of the evaluation is to check whether the given model is giving the current measures for the diagnosis of MI using MRI. The normal heart MRI passes through phase I for segmentation and experimented through phase II for feature selection and extraction. Based on the experimental evaluation, no features were found for volume calculation. So, it is clearly states that the proposed model is working well for the normal heart.

## 8.3. Statistical Evaluation

Statistical analysis is the component for analyzing the dataset. The main purpose of the statistical evaluation is to highlight the IAAP proposal.

### 8.3.1.Mean Squared Error

Statistical based evaluation had been done for the IAAP approach for estimating the Mean Squared Error (MSE). Comparing the images which have been restored requires the quality analysis. The MSE is the commonly used method for image quality analysis. MSE measures the average squares of error. Below equation explains the MSE for comparing the input images and the ground truth images.

$$MSE = \frac{1}{n}\sum_{i=1}^{n}(x_i - y_i)^2 \quad (9)$$

Where $x_i$ is the value returned by the model, n is the number of input data points, $y_i$ is the actual image data i. Table 8 illustrates the MRI frames, MSE, elapsed time and manual time taken by the experts based on 110 training samples.

**Table 8: Statistical evaluation based on training dataset on MSE**

| S. No. | Patient Number | MRI frames | Mean Squares Error | Elapsed Time | Manual Time |
|---|---|---|---|---|---|
| 1. | Patient 1 | 11 | 0.6409 | 3.50 seconds | 20 Minutes |
| 2. | Patient 2 | 50 | 0.3498 | 4.59 seconds | 20 Minutes |
| 3. | Patient 3 | 25 | 0.7947 | 3.36 seconds | 20 Minutes |
| . | . | . | . | . | . |
| . | . | . | . | . | . |
| 108. | Patient 108 | 25 | 0.7947 | 3.36 seconds | 20 Minutes |
| 109. | Patient 109 | 18 | 0.5302 | 3.34 seconds | 20 Minutes |
| 110. | Patient 110 | 20 | 0.6978 | 3. 50 seconds | 20 Minutes |
| Average | | | 0.61122 | 3.601364 seconds | 20 Minutes |

Table 9 illustrates the MRI frames, MSE, elapsed time and manual time by the experts based on 40 testing samples.

**Table 9: Statistical evaluation based on testing dataset on MSE**

| S. No. | Patient Number | MRI frames | Mean Squares Error | Elapsed Time | Manual Time |
|---|---|---|---|---|---|
| 1. | Patient 111 | 26 | 0.4165 | 3.15 seconds | 20 Minutes |
| 2. | Patient 112 | 60 | 0.3278 | 2.98 seconds | 20 Minutes |
| 3. | Patient 113 | 45 | 0.6757 | 3.36 seconds | 20 Minutes |
| . | . | . | . | . | . |
| . | . | . | . | . | . |
| 38. | Patient 148 | 28 | 0.4327 | 3.05 seconds | 20 Minutes |
| 39. | Patient 149 | 25 | 0.4025 | 3.26 seconds | 20 Minutes |
| 40. | Patient 150 | 20 | 0.5102 | 4.05 seconds | 20 Minutes |
| Average | | | 0.65833 | 3.552065 Seconds | 20 Minutes |

### 8.3.2.Structural Similarity Index

The Structural Similarity Index (SSI) is a metrics used for measuring the comparative results of the two images [44]. One is the reference image and the other one is the proposed image. The SSI is based on the visibility of the image structures.

**Table 10: Structural Similarity Index (Training)**

| Patient Number | Structural Similarity Index |
|---|---|
| Patient 1 | 97.8 |
| Patient 2 | 98.9 |
| Patient 3 | 99.2 |
| . | . |
| . | . |
| Patient 108 | 98.6 |
| Patient 39 | 99.2 |
| Patient 110 | 98.6 |

Table 10 shows the structural similarity index for the 110 training samples. Table 11 shows the structural similarity index of the 40 testing samples.

**Table 11: Structural Similarity Index (Testing)**

| Patient Number | Structural Similarity Index |
|---|---|
| Patient 111 | 98.7 |
| Patient 112 | 99.1 |
| Patient 113 | 98.9 |
| . | . |
| . | . |
| Patient 148 | 98.9 |
| Patient 149 | 98.5 |
| Patient 150 | 99.3 |

**Table 12: Scar volume comparison based on proposed model and medical experts**

| S. No. | Proposed Predictor Model (IAAP) | Medical Expert Prediction | Difference |
|---|---|---|---|
| 1 | 62.4 | 75 | 12.6 |
| 2 | 78.3 | 75 | 3.3 |
| 3 | 35.1 | 50 | 14.9 |
| 4 | 27.5 | 50 | 22.5 |
| 5 | 37.9 | 50 | 12.1 |
| 6 | 65.8 | 75 | 9.2 |
| 7 | 79.4 | 76 | 3.4 |
| 8 | 25.4 | 25 | 0.4 |
| 9 | 56.7 | 75 | 18.3 |
| 10 | 78.5 | 76 | 2.5 |
| 11 | 55.3 | 75 | 19.7 |
| 12 | 32 | 50 | 18 |
| 13 | 45.8 | 50 | 4.2 |
| 14 | 65.5 | 75 | 9.5 |
| 15 | 34.7 | 50 | 15.3 |
| 16 | 38.6 | 50 | 11.4 |
| 17 | 27.5 | 50 | 22.5 |
| 18 | 37.9 | 50 | 12.1 |
| 19 | 65.8 | 75 | 9.2 |
| 20 | 55.3 | 75 | 19.7 |
| 21 | 32 | 50 | 18 |
| 22 | 45.8 | 50 | 4.2 |
| 23 | 65.5 | 75 | 9.5 |
| 24 | 34.7 | 50 | 15.3 |
| 25 | 38.6 | 50 | 11.4 |
| 26 | 37.6 | 50 | 12.4 |
| 27 | 27.5 | 50 | 22.5 |
| 28 | 37.9 | 50 | 12.1 |
| 29 | 65.8 | 75 | 9.2 |
| 30 | 55.3 | 75 | 19.7 |
| 31 | 35.1 | 50 | 14.9 |
| 32 | 27.5 | 50 | 22.5 |
| 33 | 37.9 | 50 | 12.1 |
| 34 | 65.8 | 75 | 9.2 |
| 35 | 65.5 | 75 | 9.5 |
| 36 | 34.7 | 50 | 15.3 |
| 37 | 32.6 | 50 | 17.4 |
| 38 | 29.6 | 50 | 11.4 |
| 39 | 27.5 | 50 | 20.4 |
| 40 | 37.9 | 50 | 12.1 |

Table 12 shows the scar volume comparison based on the proposed model and the medical expert's results. The differences between the proposed model and the medical expert's results are also shown which are evaluated based on the confusion matrix on 40 testing

samples with SVM, KNN, NN and Decision tree. The results based on the SVM, KNN and Decision tree are given below.

### 8.3.3. Support Vector Machine Classification

Support Vector Machine (SVM) is a linear model for the regression and the classification problem [54]. SVM can solve both the linear and non-linear problems. The basic idea behind the SVM is to create the line which is called the linear line which separates the dataset into various classes. In this research work, the SVM takes the scar volume of 40 samples received through the proposed model as the input and outputs the line which separates the classes. So, the main risk is to find the line which is used to separate the classes. The SVM finds the line closer to both classes and separates the classes based on the line is the support-vector. The distance between the lines is calculated. The distance is named as the margin. The computation between the two planes is the hyperplane. The maximum margin is the optimal hyperplane. The SVM takes the decision based on the optimal hyperplane.

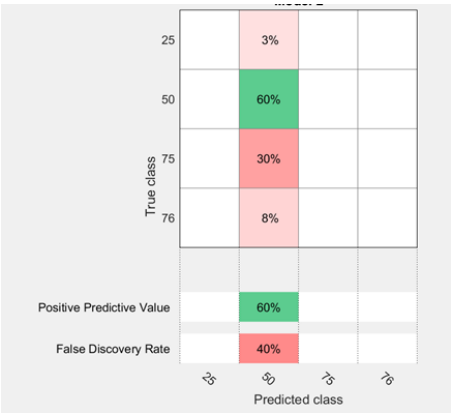


**Fig 25: Confusion matrix based on the SVM**

The confusion matrix for the SVM on the predictor model and the medical expert's results based on the volume of the scar is shown in Fig 25. The training time for the SVM is around 2.203 sec. The positive predictive value of the SVM based on the predictor class is 60% and the false discovery rate is 40%. The result reveals that the SVM can't able to find the

best optimal hyperplane based on the volume of the predictor model and medical expert's results.

### 8.3.4. K-Nearest Neighbors (KNN) Classification

K-Nearest Neighbors (KNN) are also used for the regression prediction as well as for the classification problems [55]. KNN is the supervised learning technique. KNN captures the information based on the training dataset and classifies new dataset based on the similarity. There are various distance functions, but the most commonly used distance function is the Euclidean distance which finds the distance between the new sample and the trained model.

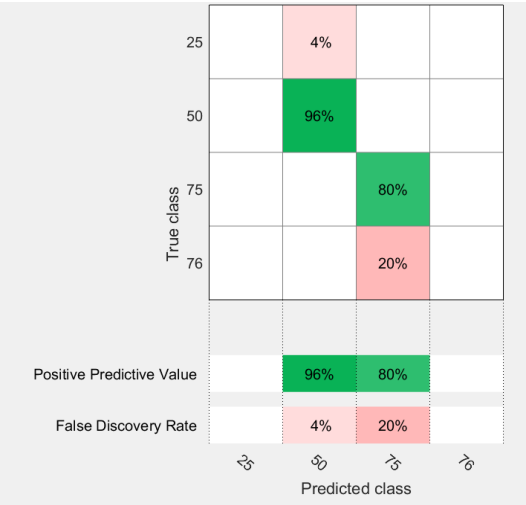


**Fig 26: Confusion matrix based on the KNN**

The confusion matrix for the KNN on the predictor model and the medical expert's results based on the volume of the scar is shown in Fig 26. The positive predictive value of the KNN based on the predictor class is 96% and the false discovery rate is 4%.

### 8.3.5. Decision Tree Classification

Confusion matrix has information about actual classification and prediction classification. Performance is calculated using the volume data of the proposed result and the expert's result. The confusion matrix includes the decision tree algorithm for small decision making. The decision tree classification and prediction training speed is fast when compared with the SVM and KNN but requires minimal tuning. The proposed model based

on the volume has been passed on to the decision tree algorithm to produce the confusion matrix along with the sensitivity, specificity and accuracy.

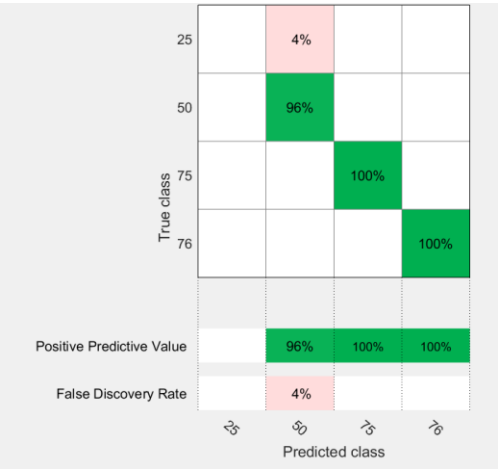


**Fig 27: Confusion matrix based on decision tree**

Fig 27 shows the true positive rates and false-negative rates. The positive predictive rate is 96% and the false discovery rate is 4%. The evaluation method for the confusion matrix is error rate and accuracy. The equation for the error rate and the confusion matrix are given below

$$Error\ Rate = \frac{False\ Positive + False\ Negative}{Positive + Negative} \tag{10}$$

Equation (10) explains the error rate calculation based on the total number of two incorrect predictions divided by a total number of the dataset.

$$Accuracy = \frac{(True\ Positive + True\ Negative)}{Positive + Negative} \tag{11}$$

Equation (11) explains, the accuracy calculation based on the total number of two correct predictions divided by the total number of the dataset.

**Table 13: Performance Evaluation of various classification algorithm**

| Classification Algorithms | Error Rate | Accuracy |
|---|---|---|
| SVM | 0.4 | 60% |
| KNN | 0.1 | 90% |
| Decision Tree | 0.03 | 97.5% |

Table 13 depicts the performance evaluation on SVM, KNN and decision tree based on classification. The performance evaluation contains the error rate and accuracy. The result clearly shows that the decision tree yields good result based on all the performance rather than the other three algorithms.

### 8.3.6. Feed Forward Neural Network Classification

The proposed model has two-layered FFNN with sigmoid hidden neurons and the linear output neurons which can fit the multidimensional problem in mapping, and the data consistent and enough neurons in hidden layers. The network is trained using the Levenberg-Marquardt backpropagation algorithm. Fig 28 shows the two-layered FFNN with 10 hidden layers.

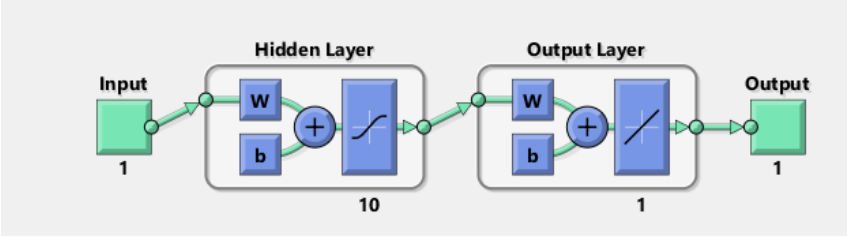


**Fig 28: Two-layered feed-forward network**

The input predictor model for the fitting problem is a 40 x 1 matrix which represents the static data of 40 samples of 1 element. There are 3 kinds of samples included, one is the training network presented to the network for the training and based on the error the network will be adjusted. The second one is the validation used to measure network generalization which halts training when an improvement in the generalization gets stopped. The final one is the testing stage did not affect the training which provides the network performance during training. The testing samples in the proposed model is randomly divided into 70% of training, 15% of validation and 15% of testing which indicates 28 samples of training, 6 samples of validation and 6 samples of testing.

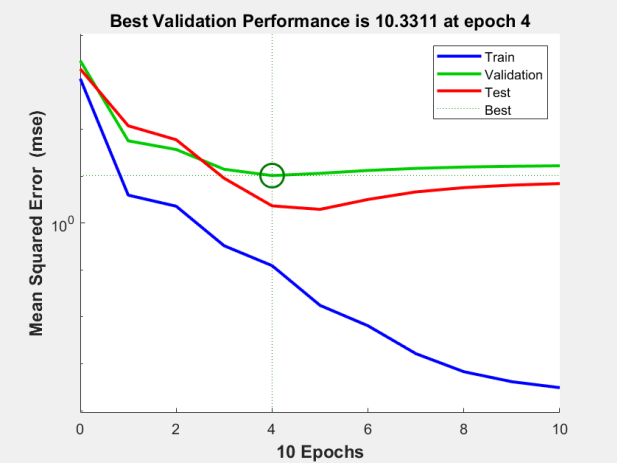


**Fig 29: Best validation performance**

Fig 29 shows the best validation performance of the volume classification based on 40 samples. The best validation for the volume classification stops at epoch 4. In general, the error will be reduced after the epoch is more. But the validation dataset starts by increasing while the network starts overfitting the training samples. The default dataset training stops after every six increases in the validation error. The best validation performance is taken from the lowest validation error.

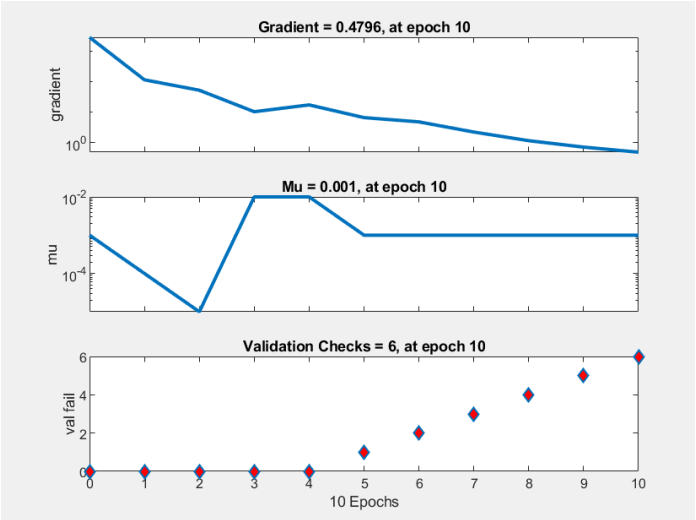


**Fig 30: Neural Network training state**

Fig 30 shows the gradient variation coefficient with the epoch numbers. The gradient value decreases when the epoch increases in the NN training stage. The NN weight is adjusted using the MU. The value ranges $from\ 10^{-2}\ to\ 10^{-6}$. Validation check controls the

performance of the non-trained data. The last value of gradient coefficient at the epoch 10 is 0.4796 which is near to zero. If the value of the gradient coefficient value is decreased which means the better network training and testing. In the proposed research work, the gradient coefficient value is decreased with increase in epoch value which also includes the gradient and validation check parameters which are used for training and testing the FFNN.

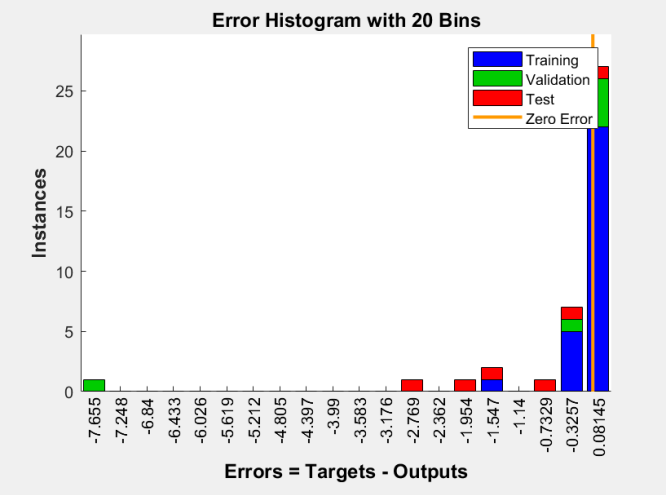


**Fig 31: Error histogram**

Fig 31 explains the error histogram of NN which is calculated based on the target value subtracted from the output value. Bins are the vertical bar in the graph. The total error starts from the range of -7.655 from the left to 0.08145 to the left. The range of error in the graph is divided into 20 smaller bins. Every vertical bar represents the samples of the dataset in the bins. The error histogram is an additional verification for the performance of the network. The blue color in the figure shows the training dataset, green shows the validation, red for testing the dataset and finally, the orange line shows the zero error. The proposed model error histogram is close to zero.

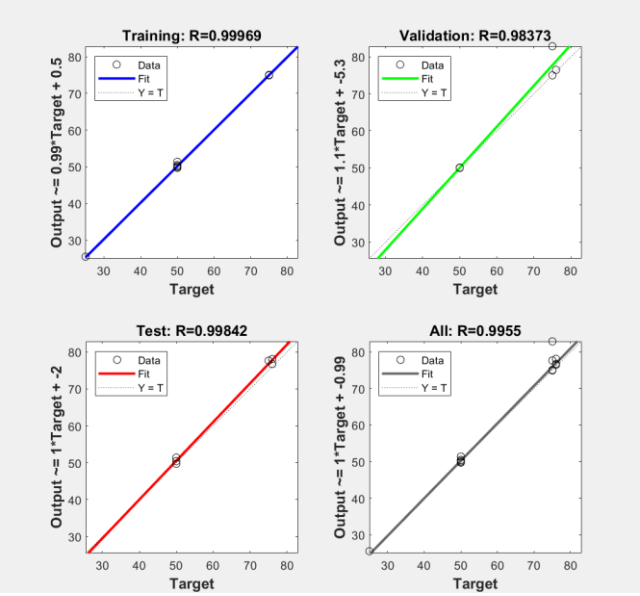


**Fig 32: Regression Plots**

Fig 32 shows the four plots of the regression of the FFNN which is training, validation, testing and finally all result. In general, the regression plot has four graphs. The graph shows whether the dataset is fitted right on the line which indicates the NN correct structure. The figure specifies the data, fitness and accuracy. The ring is the data, the dotted line is the accuracy and the colored line is the fitness. The value of R indicates the correlation between the output value and the targeted value. The training R-value is 0.999, validation R-value is 0.983, the testing R-value 0.998 and finally, altogether R-value is 0.995.

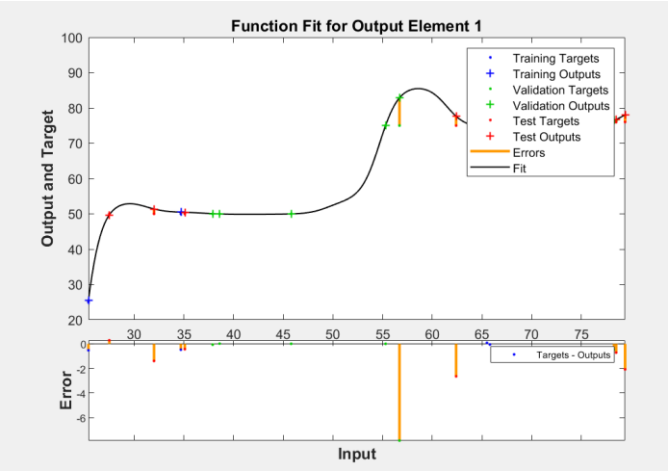


**Fig 33: Neural Network training fit**

Fig 33 shows the NN training fit, blue dot represent the training targets, blue colored cross represents the training outputs, green dot represents the validation targets, green-colored cross specifies the validation outputs, red dot represents the test targets, red-colored cross represents the test outputs, orange line represents the errors and finally the black line represents the fit. The hidden layers have been reduced as 5 and checked. The result of 5 hidden layers for the classification based on the scar volume has reduced the accuracy rate of 95.5%.

### 8.3.7. Performance of the Proposed Model (IAAP)

The proposed model is based on the five phases. Based on the phases the model has been build and then classified based on the 4 classes and predicted whether the patient leads to arrhythmia.

| Proposed Phases | Patient 1 | Patient 2 | Patient 3 |
|---|---|---|---|
| Phase I (Median Filtering) | 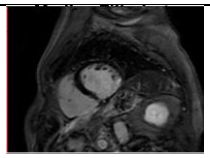 | 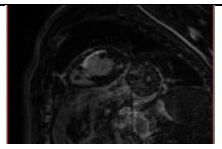 | 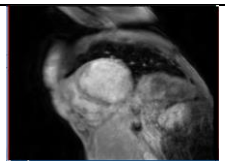 |
| Phase II (Morphological Filtering and FCM) | 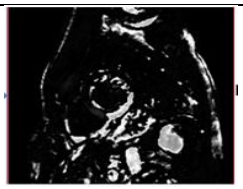 | 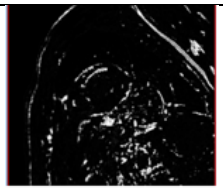 | 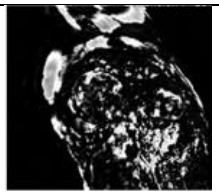 |
| Phase III (Gray Thresholding and Region Growing) | | 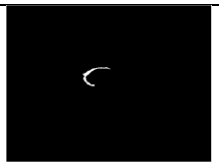 | 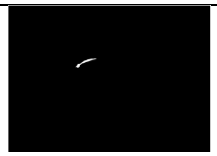 |
| Phase IV (Decision Tree) | 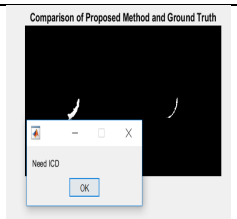 | 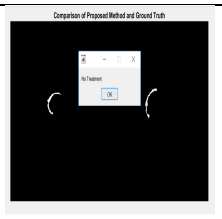 | 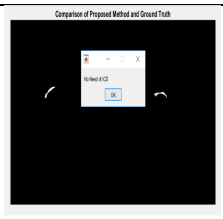 |

**Fig 34: Overall Performance of the Proposed Model**

Fig 34 shows the overall performance of the proposed model which is tested based on the 3D enhanced myocardial infarcted MRI.

### 8.3.8. Performance Evaluation on Systole with Ground Truth Images

The most common approach of finding the scar is based on the diastolic position of the MRI. Identification of scar in the systolic position is very difficult. But the proposed model can identify the scar region even in the systolic position also.

| Patient No | Frames no. 20 of Systole to Diastole | Proposed Model and Ground Truth Images |
|---|---|---|
| Patient 1 | | |
| Patient 2 | 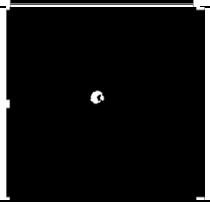 | 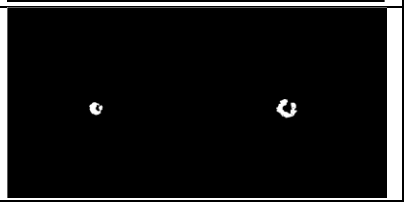 |

**Fig 35: Testing Based on Systole with Ground Truth**

Fig 35 shows the identification of scar region in the systolic position which is also compared with the ground truth image. Patient 1 and patient 2 at the systolic position in frame 20 shows very small scar region which can also be identified through the proposed model. So, the proposed model yields good result even in the systolic position also.

**Table 14: Statistical evaluation based on training dataset on MSE**

| S. No. | Patient Number | MRI frames | Mean Squares Error | Elapsed Time | Manual Time |
|---|---|---|---|---|---|
| 1. | Patient 1 | 11 | 0.6409 | 3.50 seconds | 20 Minutes |
| 2. | Patient 2 | 50 | 0.3498 | 4.59 seconds | 20 Minutes |
| 3. | Patient 3 | 25 | 0.7947 | 3.36 seconds | 20 Minutes |
| 4 | Patient 4 | 20 | 0.6235 | 3.10 seconds | 20 Minutes |
| 5 | Patient 5 | 20 | 0.6472 | 3.25 seconds | 20 Minutes |
| 6. | Patient 6 | 25 | 0.7947 | 3.36 seconds | 20 Minutes |
| 7. | Patient 7 | 18 | 0.5302 | 3.34 seconds | 20 Minutes |
| 8. | Patient 8 | 20 | 0.6978 | 3.35 seconds | 20 Minutes |
| 9. | Patient 9 | 28 | 0.7925 | 4.56 seconds | 20 Minutes |
| 10. | Patient 10 | 43 | 0.7120 | 3.16 seconds | 20 Minutes |
| Average | | | 0.65833 | 3.557 seconds | 20 Minutes |

Table 14 shows the statistical report of training only 10 samples and the means squared error of 10 patients with an elapsed time of the proposed model and the manual timings are listed. Table 15 shows the statistical evaluation based on 5 samples and the mean squared error along with the elapsed time and manual time are listed. The result of the less number of training and testing samples also reveals that the proposed model is working good for small dataset but yields little variation in the mean squared error.

**Table 15: Statistical evaluation based on testing dataset on MSE**

| S. No. | Patient Number | MRI frames | Mean Squares Error | Elapsed Time | Manual Time |
|---|---|---|---|---|---|
| 1. | Patient 11 | 26 | 0.4165 | 3.15 seconds | 20 Minutes |
| 2. | Patient 12 | 60 | 0.3278 | 2.98 seconds | 20 Minutes |
| 3. | Patient 13 | 45 | 0.6757 | 3.36 seconds | 20 Minutes |
| 4. | Patient 14 | 28 | 0.4327 | 3.05 seconds | 20 Minutes |
| 5. | Patient 15 | 25 | 0.4025 | 3.26 seconds | 20 Minutes |
| Average | | | 0.751733 | 3.16 | 20 |

# DISCUSSION

The study included 150 samples of MI patients, where the proposed IAAP model demonstrated positive results. The IAAP approach was extended to non-ischemic samples as well. This approach was developed to provide an efficient computational model for an early prediction of arrhythmia using MI in MRI. This model proved to be efficient due to the fact that existing research for the prediction of arrhythmia mostly revolved around ECG results. Utilizing integrated image-based computational model for the prognosis of an arrhythmia patient highlighted the progressive nature of this research study.

For the purpose of this study, the IAAP approach contributed in terms of identifying high-risk arrhythmia patients, which could be used to avoid unnecessary implementation of ICD. To address clinical needs, the current approach was considered as one of the best models for an early prediction of arrhythmia based on MI in MRI.

# 9. CONCLUSIONS

Myocardial infarction disease is one of the most predominant causes of deaths worldwide. Early detection of scaring in myocardial infarcted patient could potentially prevent arrhythmia. The current research work applied a hybrid model for an early prediction of arrhythmia using myocardial infarction magnetic resonance imaging. This model consisted of five stages basis which, the following conclusion was drawn.

The classification model was evaluated based on a referential classifier using levenberg marquardt neural network, which portrayed 99.5% accuracy. The results clearly indicated the proposed model as ideal for the early prediction of an arrhythmia patient.

The current research has been conducted using five stages which involved measuring the volume of a scar in the myocardial infarcted patients for an early prediction of arrhythmia. Future studies could be more in-depth, which involves shape analysis of the left ventricle in a short-axil view based on the age and sex of the participants. Based on the proposed framework, a tool could be developed, potentially acting as a second opinion for medical experts for faster analysis.

# REFERENCES


1. Libby P, “Mechanisms of acute coronary syndromes and their implications for therapy”, New England Journal of Medicine, vol. 368, no.21, pp. 2004-2013, 2013.
2. Antonino M. Grande and Alessandro Mazzola,” Mechanical Complications of Acute Myocardial Infarction”, Operative Techniques and Recent Advances in Acute Care and Emergency Surgery, pp. 583-593, 2019.
3. Justine Bhar-Amato, William Davies and Sharad Agarwal, “Ventricular arrhythmia after acute myocardial infarction: ‘The perfect storm’, Arrhythmia and electrophysiology review, vol 6, no. 3, pp. 134-139, 2017.
4. Kawaji K, Tanaka A, Patel MB, Wang H, Maffessanti F, Ota T, and Patel AR,”3D late gadolinium enhanced cardiovascular MR with CENTRA-PLUS profile/view

ordering: Feasibility of right ventricular myocardial damage assessment using a swine animal model", in Magnetic Resonance Imaging, vol. 39, pp. 7-14, 2017.

5. Belaroussi, J. Milles, S. Carme, Y. M. Zhu, and H. Benoit-Cattin, "Intensity non-uniformity correction in MRI: existing methods and their validation," Medical Image Analysis, vol. 10, no. 2, pp. 234–246, 2006.
6. U. Vovk, F. Pernuš, and B. Likar, "A review of methods for correction of intensity inhomogeneity in MRI," IEEE Transactions on Medical Imaging, vol. 26, no. 3, pp. 405–421, 2007.
7. M. A. Balafar, A. R. Ramli, M. I. Saripan, and S. Mashohor, "Review of brain MRI image segmentation methods," Artificial Intelligence Review, vol. 33, no. 3, pp. 261–274, 2010.
8. P. Coupe, P. Yger, S. Prima, P. Hellier, C. Kervrann, and C. Barillot, "An optimized blockwise nonlocal means denoising filter for 3-D magnetic resonance images," IEEE Transactions on Medical Imaging, vol. 27, no. 4, pp. 425–441, 2008.
9. H. Liu, C. Yang, N. Pan, E. Song, and R. Green, "Denoising 3D MR images by the enhanced non-local means filter for Rician noise," Magnetic Resonance Imaging, vol. 28, no. 10, pp. 1485–1496, 2010.
10. J. V. Manjón, P. Coupé, L. Martí-Bonmatí, D. L. Collins, and M. Robles, "Adaptive non-local means denoising of MR images with spatially varying noise levels," Journal of Magnetic Resonance Imaging, vol. 31, no. 1, pp. 192–203, 2010.
11. J. Hu, Y. Pu, X. Wu, Y. Zhang, and J. Zhou, "Improved DCT-based nonlocal means filter for MR images denoising," Computational and Mathematical Methods in Medicine, vol. 2012, Article ID 232685, 14 pages, 2012.
12. R. P. Velthuizen, J. J. Heine, A. B. Cantor, H. Lin, L. M. Fletcher, and L. P. Clarke, "Review and evaluation of MRI nonuniformity corrections for brain tumor response measurements," Medical Physics, vol. 25, no. 9, pp. 1655–1666, 1998.
13. J. B. Arnold, J.-S. Liow, K. A. Schaper et al., "Qualitative and quantitative evaluation of six algorithms for correcting intensity nonuniformity effects," NeuroImage, vol. 13, no. 5, pp. 931–943, 2001.

14. Z. Hou, “A review on MR image intensity inhomogeneity correction,” International Journal of Biomedical Imaging, vol. 2006, 11 pages, 2006.
15. B. Belaroussi, J. Milles, S. Carme, Y. M. Zhu, and H. Benoit-Cattin, “Intensity non-uniformity correction in MRI: existing methods and their validation,” Medical Image Analysis, vol. 10, no. 2, pp. 234–246, 2006.
16. L. O. Hall, A. M. Bensaid, L. P. Clarke, R. P. Velthuizen, M. S. Silbiger, and J. C. Bezdek, “A comparison of neural network and fuzzy clustering techniques in segmenting magnetic resonance images of the brain, Neural Networks”, IEEE Transactions on, vol. 3, no. 5, pp. 672-682, 1992.
17. S. Shen, W. Sandham, M. Granat, and A. Sterr, "MRI Fuzzy Segmentation of Brain Tissue Using Neighbourhood Attraction with Neural-Network Optimization", IEEE Transaction on Information Technology in Biomedicine, vol. 9, no. 3, pp. 459-467, 2005.
18. L. L. He, and I. R. Greenshields, "An MRF spatial fuzzy clustering method for fMRI SPMs", Biomedical Signal Process Control, vol. 3, no. 4, pp. 327-333, 2008.
19. Y. Xia, D. G. Feng, T. J. Wang, R. C. Zhao, and Y. N. Zhang, "Image segmentation by clustering of spatial patterns", Pattern Recognition Letters, vol. 28, no. 12, pp. 1548-1555, 2007.
20. D. Q. Zhang, and S. C. Chen, "A novel kernelized fuzzy C-means algorithm with application in medical image segmentation", Artificial Intelligence in Medicine, vol. 32, no. 1, pp. 37-50, 2004.
21. D. Graves, and W. Pedrycz, "Kernel-based fuzzy clustering and fuzzy clustering: A comparative experimental study", in Fuzzy Sets and System, vol. 161, no. 4, pp. 522-543, 2010.
22. S. C. Chen, and D. Q. Zhang, "Robust image segmentation using FCM with spatial constraints based on new kernel-induced distance measure", IEEE Transactions on Systems, Man, and Cybernetics, vol. 34, no. 4, pp. 1907-1916, 2004.

23. H. Y. Li, V. Bochko, T. Jaaskelainen, J. Parkkinen, and I. F. Shen, "Kernel-based spectral color image segmentation", Journal of the Optical Society of America A, Optics, Image Science, vol. 25, no. 11, pp. 2805-2816, 2008.
24. B. Zhao, J. Kwok, and C. Zhang, "Multiple kernel clustering", Proc. SIAM International Conference on Data Mining, pp. 638-649, 2009.
25. Q. Li, N. Mitianoudis, and T. Stathaki, "Spatial kernel K-harmonic means clustering for multi-spectral image segmentation", IET Image Processing, vol. 1, no. 2, pp. 156-167, 2007.
26. K. Muneeswaran, L. Ganesan, S. Arumugam, and K. R. Soundar, "Texture image segmentation using combined features from spatial and spectral distribution", Pattern Recognit. Letter, vol. 27, no. 7, pp. 755-764, 2006.
27. A. Guerrero-Curieses, J. L. Rojo-Alvarez, P. Conde-Pardo, I. Landesa-Vazquez, J. Ramos-Lopez, and J. L. Alba-Castro, "On the performance of kernel methods for skin color segmentation", EURASIP Journal on Advanced in Signal Processing, vol. 2009, pp. 1-13, 2009.
28. J. C. Bdezek, Pattern Recognition with Objective Fuzzy Algorithms, Plenum press, New York, 1981.
29. K. Sathiyasek, S. Karthick and P. Kanniya, 'The survey on various clustering technique for image segmentation," International Journal of Advanced Research in Electronics and Comm. Eng. (IJARECE), vol. 3, no. I, pp. 47-50, 2014.
30. K. Honda and H. Ichihashi, "Regularized linear fuzzy clustering and probabilistic PCA mixture models," IEEE Trams. Fuzzy Systems, vol. 13, no. 4, pp. 508-516, 2005.
31. P. Coupe, P. Yger, S. Prima, P. Hellier, C. Kervrann, and C. Barillot, “An optimized blockwise nonlocal means denoising filter for 3-D magnetic resonance images,” IEEE Transactions on Medical Imaging, vol. 27, no. 4, pp. 425–441, 2008.
32. H. Liu, C. Yang, N. Pan, E. Song, and R. Green, “Denoising 3D MR images by the enhanced non-local means filter for Rician noise,” Magnetic Resonance Imaging, vol. 28, no. 10, pp. 1485–1496, 2010.

33. J. V. Manjón, P. Coupé, L. Martí-Bonmatí, D. L. Collins, and M. Robles, “Adaptive non-local means denoising of MR images with spatially varying noise levels,” Journal of Magnetic Resonance Imaging, vol. 31, no. 1, pp. 192–203, 2010.
34. J. Hu, Y. Pu, X. Wu, Y. Zhang, and J. Zhou, “Improved DCT-based nonlocal means filter for MR images denoising,” Computational and Mathematical Methods in Medicine, vol. 2012, Article ID 232685, 14 pages, 2012.
35. R. D. Nowak, “Wavelet-based rician noise removal for magnetic resonance imaging,” IEEE Transactions on Image Processing, vol. 8, no. 10, pp. 1408–1419, 1999.
36. C. S. Anand and J. S. Sahambi, “Wavelet domain non-linear filtering for MRI denoising,” Magnetic Resonance Imaging, vol. 28, no. 6, pp. 842–861, 2010.
37. M. E. Alexander, R. Baumgartner, A. R. Summers et al., “A wavelet-based method for improving signal-to-noise ratio and contrast in MR images,” Magnetic Resonance Imaging, vol. 18, no. 2, pp. 169–180, 2000.
38. J.-H. Xue, A. Pizurica, W. Philips, E. Kerre, R. Van De Walle, and I. Lemahieu, “An integrated method of adaptive enhancement for unsupervised segmentation of MRI brain images,” Pattern Recognition Letters, vol. 24, no. 15, pp. 2549–2560, 2003.
39. Zhong Qu andLi Hang "Research on Iimage Segmentation Based on the Improved Otsu Algorithm.", 2010.
40. J. Gong, L. Li, and W. Chen, “Fast recursive algorithms for two-dimensional thresholding,” Pattern Recognition, vol. 31, no. 3, pp. 295–300, 1998.
41. S. Goyal, “Region growing Adaptive Contrast Enhancement of Medical MRI Images,” J. Glob. Res. Computer Science., vol. 2, no. 7, pp. 93–95, 2011.
42. M. G. Oghli, A. Fallahi, and M. Pooyan, “Automatic region growing method using GSmap and spatial information on ultrasound images,” in 2010 18th Iranian Conference on Electrical Engineering, pp. 35–38, 2010.
43. A. Girdhar, “Region Based Adaptive Contrast Enhancement of Medical Ultrasound Images,” pp. 750–753, 2015.

44. Chen Chenglong, Ni Jiangqun, Huang Jiwu, "Blind Detection of Median Filtering in Digital Images: A Difference Domain Based Approach", Image Processing IEEE Transactions, vol. 22, pp. 4699-4710, 2013.
45. C. S. Anand and J. S. Sahambi, “Wavelet domain non-linear filtering for MRI denoising,” Magnetic Resonance Imaging, vol. 28, no. 6, pp. 842–861, 2010.
46. Chyntia Raras, Ajeng Widiawati, and Kuat Indartono, “ Double morphological segmentation for increasing performance of signature classification using machine learning technique”, in International Conference on Information Technology, Information Systems and Electrical Engineering, pp. 94-99, 2018.
47. Y. Yang, and S. Huang, "Image segmentation by fuzzy c-means clustering algorithm with a novel penalty term", Comput. Informatics, vol. 26, pp. 17-31, 2012.
48. Md. Abu Bakr Siddique, Rezoana Bente Arif, and Mohammad Mahmudur Rahman Khan, “ Digital image segmentation in Matlab: A brief study on OTSU’s image thresholding”, in International Conference on Innovation in Engineering and Technology, pp. 1-5, 2018.
49. J. C. Bdezek, Pattern Recognition with Objective Fuzzy Algorithms, Plenum press, New York, 1981.
50. R. Adams and L. Bischof, "Seeded Region Growing," IEEE Transaction on Pattern Analysis and Machine Intelligence, vol. 16, pp. 641-647, 1994.
51. Brijesh N. Shah, Satish K Shah, and Y. P. Kosta, “A seeded region growing algorithm for spot detection in medical image segmentation”, in International Conference on Image Information Processing, pp. 1-4, 2011.
52. Monica Madhukar, Sos Agaian and Anthony T. Chronopoulos, "New decision support tool for acute lymphoblastic leukemia classification", in IS&T /SPIE Electronic Imaging. International Society for Optics and Photonics, Vol. 8295, pp. 1-12, 2012.
53. CG Fonseca, M Backhaus, DA Bluemke, RD Britten, JD Chung, BR Cowan, ID Dinov, JP Finn, PJ Hunter, AH Kadish, DC Lee, JAC Lima, P Medrano-Gracia, K Shivkumar, A Suinesiaputra, W Tao, and AA Young, ”The Cardiac Atlas Project –

An imaging database for computational modeling and statistical atlases of the heart," Bioinformatics, vol.27, no.16, pp. 2288–2295, 2011.

54. M. M. Rahman, S. K. Antani, and G. R. Thoma, "A medical image retrieval framework in correlation enhanced visual concept feature space," in Proc. 22nd IEEE Int. Symp. Comput.-Based Med. Syst., pp. 1–4, 2009.
55. B.V. Dasarathy, "Nearest Neighbor (NN) Norms: NN pattern classification techniques", in CA:IEEE Computer Society Press, 1990.

# LIST OF PUBLICATIONS

## Journals

1. R.Merjulah and Chandra J., "Experimental Evaluation of image segmentation for heart images", in International Journal of Computer Aided Engineering and Technology, Inderscience. (**Scopus Indexed**) (D.O.I: 10.1504/IJCAET.2021.10024945).
2. R.Merjulah and Chandra J., "Automated Segmentation and Feature Extraction for Myocardial Ischemia", in Springer Nature Applied Sciences. (**Accepted for Publication**).
3. R.Merjulah and Chandra J., "An Integrated Segmentation Technique for Myocardial Ischemia Using MRI", in Pattern Recognition and Image Analysis (Springer) (**Accepted for Publication**)(**Scopus Indexed**)
4. R.Merjulah and Chandra J., "Machine Learning based Prediction Analytics for Cardiac Arrhythmia using MRI" in ACM Transaction on Computer Systems (**Scopus Indexed**) (Under Review)

## Conferences

1. R.Merjulah and Chandra J., "Segmentation technique for medical image processing: A survey" in International Conference on Inventive Computing and Informatics (ICICI), IEEE, Hotel Arcadia, Coimbatore, Nov 23-24, 2017, pp. 1055-1061. **ISBN:** 978-1-5386-4031-9. (DOI: 10.1109/ICICI.2017.8365301) (**Scopus Indexed**).

2. R.Merjulah and Chandra J., “Medical Image Classification Using MRI: An Investigation”, in Proceedings of the International Conference on (ISMAC) SPRINGER, SCAD Institute of Technology, Palladam, Tiruppur, May 16-17, 2018, pp. 1135-1146, **ISBN:** 978-3-030-00665-5 (**Scopus Indexed**).
3. R.Merjulah and Chandra J., “An Integrated Method for Myocardial Ischemia Segmentation Using MRI”, in Proceedings of the International Conference on Digital Image and Signal Processing, St. Hughs College, Oxford University, Oxford, Apr. 29-30, 2019, **ISBN**: 978-1-912532-05-6 (**Scopus Indexed**).
4. R.Merjulah and Chandra J., “Experimental Evaluation of image segmentation for heart images”, in proceedings of International Conference on Sustainable Advanced Computing and Statistical Technique, 2019.

## Book Chapters

1. R.Merjulah and Chandra J., “Medical Image Classification Using MRI: An Investigation”, in Proceedings of the International Conference on ISMAC in computational Vision and Bio-Engineering 2018 (ISMAC-CVB), SPRINGER, pp. 1135-1146, 2019. **ISBN** 978-3-030-00665-5. (**DOI**: 10.1007/978-3-030-00665-5_108) (**Scopus Indexed**).
2. R.Merjulah and Chandra J., “Classification of Myocardial Ischemia in Delayed Contrast Enhancement Using Machine Learning” in Intelligent Data Analysis for Biomedical Applications: Challenges and Solutions”, ELSEVIER, pp. 209-233, 2019. **ISBN**: 9780128155530 (**Scopus Indexed**).